Butterfly Patterns: Small-Angle Neutron Scattering from Deuterated Mobile Chains in a Randomly Cross-Linked Polystyrene Network

A. Ramzi,*,† F. Zielinski,*,† J. Bastide,‡ and F. Boué†

Laboratoire Léon Brillouin (CEA−CNRS), Centre d'Etudes, Saclay, F-91191 Gif-sur-Yvette Cedex, France, and Institut Charles Sadron (CRM−EAHP), 6 rue Boussingault, F-67083 Strasbourg Cedex, France

Received April 18, 1994; Revised Manuscript Received February 21, 1995®

ABSTRACT: The small-angle neutron scattering (SANS) was measured from networks containing deuterated un-cross-linked small chains (of molecular weights M_{WD} = 14 370 and 73 000) under uniaxial extension of ratio λ up to the maximum value before breaking ($\lambda \sim 2$). In the *isotropic state*, the scattering increases with cross-linking, in a stronger way for large M_{WD}. In the *deformed state*, the scattering, in particular its zero-q limit, varies with the direction with respect to the stretching axis. It increases in all directions, corresponding to a dilation of the sample (i.e., parallel). It decreases slightly, back to the random mixing scattering, along contracted directions (i.e., perpendicular). The isointensity contours on the two-dimensional detector have a double-winged shape, often called *butterfly patterns*. The most striking effect is the appearance and the enlargement under strain of an "intermediate regime" of scattering, characterized by a *limit curve* with a power law dependence of $I(q)$ with q. The zero-q limit, I_0, and the correlation length, ξ, vary as an apparent power law of λ. Such an effect is not predicted by the classical models of elasticity combined with random mixing, but by other models developed recently. Quantitative comparisons lead to discarding the amplification under strain of spontaneous fluctuations (Y. Rabin and R. Bruinsma), at least in its version for small deformation. We discard also a perturbation model of uncorrelated frozen fluctuations (A. Onuki) which predicts a too strong variation of $I(q)$. Considering *correlated* frozen heterogeneities and *unscreening* effects associated with the spatial separation under cross-linking and deformation of percolation-like clusters leads to a qualitative prediction of the limit curve and the power laws. The percolation exponents are larger than observed. This discussion can be extended to similar butterfly patterns observed in other permanent or temporary (entangled) networks permeated by a mobile species.

1. Introduction

The present work concerns a study of the small-angle neutron scattering (SANS) of perdeuterated linear chains dispersed in a chemical network of chains of the same chemical species, but not deuterated. Such a mixture belongs to a more general class of bicomponent mixtures which differ in the time scale of their mechanical self-relaxation: one of the components is "slow" and displays an elastic behavior; the other is "fast" and displays a mobile behavior. The mobile species can be un-cross-linked linear chains (L), as in the present case, or solvent molecules (S). The elastic species can be a chemical network (N), as here, or entangled chains (E). The system (N−L) considered in this paper resembles a polymer melt blend, where the network is replaced by long entangled chains. It is also similar to a gel, where the mobile short chains would be replaced by a solvent (N−S). Semidilute solutions (E−S) of entangled chains in the presence of a solvent would be the fourth element of the series. *All associations* display the following similar behavior: under a *dilation* of the material in a given direction, the scattering of the mixture when one component is labeled with respect to the other *increases*. If the elastic component is a permanent network, the deformation can be the increase of volume of the network (swelling) due to mixing with the mobile species or a permanent mechanical deformation.[1−3] If the elastic chains are entangled, it may be only a transient mechanical deformation.[4] In the case of uniaxial extension, of ratio λ, some directions, of angle ψ, are dilated while some are contracted (the perpendicular direction). It is found that the intensity at small q ($q \to 0$) varies with ψ. This is at variance with, for example, the form factor of a deformed particle, which tends at $q \to 0$ toward a value independent of ψ and which is proportional to the molecular weight. This variation is also in disagreement with the scattering of an interchain structure which would be affinely deformed. Because of this ψ dependence, the isointensity patterns joining cells of equal counting on the multidetector have an eight shape, often called *butterflies*, rather than an elliptical shape. Similar effects have been observed more recently on sheared polymer solutions by light scattering[5−7] and by SANS.[8]

On the theoretical side, different models are now proposed. Recently, the coupling between deformation and concentration via the concentration dependence of the moduli[9] or of the viscosity[10,11] has been predicted to provoke spontaneous anisotropic fluctuations. Previously, a picture of frozen heterogeneities, which separate under swelling or stretching, was proposed.[12] The separation of the structure was treated in the case of the vicinity to a percolation threshold. More recently, a perturbation treatment of the uncorrelated frozen heterogeneities has been proposed.[13]

In this paper, these models are analyzed and compared with our data as a function of the deformation ratio, the cross-linking density, and the molecular weight of the mobile chains. For a more detailed study, the mechanical stress of each sample, observed by SANS, has also been measured. The agreement with

* To whom correspondence should be addressed. Present address: Institut für Festkörperforschung, Forschungszentrum Jülich, D-52425 Jülich, Germany.
† Laboratoire Léon Brillouin (CEA−CNRS).
‡ Institut Charles Sadron.
® Abstract published in *Advance ACS Abstracts,* April 1, 1995.

0024-9297/95/2228-3570$09.00/0

Table 1. Characteristics of the Different Aminomethylated Polystyrene Precursors

precursor	A_{NH_2}[a]	M_{WH}[b]	C_{prep}[c]
R14	48	363 900	0.1
R15	30	335 900	0.1
F82	80	763 000	0.1
F112	79	525 000	0.1
F117	81	525 000	0.1
F146	47	426 000	0.1
F135	100	525 000	0.1

[a] Average number of monomers between two active sites. [b] Molecular weight of precursor. [c] Polystyrene concentration prior to cross-linking.

models using classical linear elasticity is shown to be incomplete. The observed power law dependence suggests an influence of a correlated frozen structure, not yet elucidated in the present case.

2. Experimental Section

Cross-Linking. Polystyrene (PS) networks were cross-linked at random in two steps.

The first step is *aminomethylation*: this step involves the fixation of NH_2 groups on narrow molecular weight distribution polystyrene chains. The NH_2 groups are assumed to react at random along the chain. A polystyrene solution is prepared in distilled dichloromethane with a fixed concentration (generally 10% g/mL) under an argon atmosphere at room temperature. A given amount, C_{phthal}, of *N*-(chloromethyl)phthalimide is added to the polystyrene solution with $SnCl_4$ as catalyst. The reaction is carried out under argon for a given time, which, together with C_{phthal}, will determine the final ratio of aminomethylation. The reaction is stopped by the addition of a small quantity of tetrahydrofuran (THF); the mixture is diluted with dichloromethane, and the polymer is precipitated into methanol and dried at room temperature. The dried polymer is then redissolved in THF with an excess of hydrazine. The reaction, which brings the NH_2 groups on the chains, is driven under reflux for approximately 10 h. The solution is subsequently filtered and the polymer precipitated twice in methanol to remove the catalyst in the presence of a base (potassium *tert*-butoxide). The parameter A, which represents an average number of monomers between two active sites, can be measured by HCl titration in a water/THF mixture. The principal characteristics of aminomethylated precursors are listed in Table 1.

The second step involves the binding together of the active sites of the chains in semidilute solution, using benzenedicarbaldehyde as the cross-linking agent. The mixture, which appears perfectly homogeneous, is poured into a mold with a Teflon frame and glass plates covered with paper. The cross-linking reaction is allowed to proceed at 60 °C for 7 days.

Finally, the gels are dried, initially at room temperature and then at gently increasing temperature, under vacuum above 100 °C up to 150 °C. Higher temperatures give rise to chain scission. The equilibrium swelling of the samples, Q_{eq}, was measured just after the gelation reaction and after drying. The values are very different: drying decreases Q_{eq} by a factor of 3−4. The reaction continues during the drying process. We do not know how to avoid this second-stage cross-linking.

Cotrapping and Posttrapping of the Deuterated Chains in the Network. We have included inside the network made of nondeuterated chains cross-linked together some deuterated chains which are not cross-linked: the contrast between labeled and nonlabeled chains enables the measurement of a SANS signal. The un-cross-linked chains remain inside the network, so they may be referred to as "trapped" chains. They may be extracted by solvent washing and display a quasi-isotropic conformation inside a deformed network in equilibrium under deformation (see below); therefore we can call them "free chains". The un-cross-linked chains may be included after fabrication of the sample by dipping the latter in a solution[2] or in a melt[1] (postreaction trapping) or during the cross-linking reaction (cotrapping). In this latter case, an earlier study showed[2] that the free chains are not cross-linked whereas the other aminomethylated chains are. One disadvantage of cotrapping is that the presence of free chains influences the cross-linking reaction, as observed from the equilibrium swelling and elastic modulus values. One advantage is that the percentage, C_D (in g/cm^3), of the free chains incorporated in the network is fixed. In posttrapping, no modification of the network is expected, but C_D is very difficult to control since it depends on M_{WD}, the duration of dipping, the cross-linking density of the network, and the concentration of the solution. The characteristics of the different cross-linked samples are presented in Table 2.

Table 2. Characteristics of the Different Cross-Linked Samples, Method of Trapping the Chains, and Swelling Results

sample	precursor	M_{WD}[a]	wt %[b]	method	Q_{eq}[c]
AR141	R14				10.35
AR142	R14	14 370	20	co-trapping	12.35
AR143	R14	73 000	20	co-trapping	12.7
AR144	R14	14 370	22.5	dipping	11.42
AR153	R15	73 000	20	co-trapping	8.6
H1201	F82	138 000	10	co-trapping	16.6
H0601	F112	751 000	10	co-trapping	13
H0730	F117	545 000	10	co-trapping	13.1
H1250	F146	73 000	28	co-trapping	13.6
H0942	F135	138 000	10	co-trapping	8.25

[a] Molecular weight of free chains. [b] Fraction of polymer incorporated in the network. [c] Equilibrium swelling ratio prior to drying.

Sample Deformation. After drying, the polystyrene samples are in the glassy state. They can be cut into strips of dimensions 7 cm × 1 cm × 0.1 cm of a very constant thickness (±1/100 mm). Following immersion in an oil bath, the samples are equilibrated at a temperature $T_1 > T_g$ ($T_g = 100$ °C, where T_g is the glass transition temperature) and then rapidly stretched in less than 1 min to an elongation ratio $\lambda = L_f/L_0$, where L_0 and L_f are the lengths before and after stretching. The samples are maintained at constant length, L_f, and constant temperature, T, for a certain time, t_R, referred to as the "relaxation time", after which they are withdrawn from the bath, thus freezing the deformation in the glassy state. The small-angle neutron scattering from the samples is then measured. After this measurement, they are reimmersed in the bath under extension and either (i) relaxed for a longer time before being requenched and *analyzed once again by SANS* or (ii) stretched at a higher λ in 10 s, relaxed for 10 min, and reanalyzed again.

At temperatures close to T_g, the time-temperature superposition principle[14,15] (Vogel−Fulcher or Williams−Landel−Ferry (WLF) law) can be applied; i.e., $t_R(T_1) \sim a_{T_1}/a_{T_2} t_R(T_2)$. a_T varies rapidly with $T - T_g$. The wait time, t_R (10 min), is generally much larger than the stretching time (10 s). The entire procedure may thus be assimilated to a step deformation.

Careful measurements of tensile force were also performed. Immediately after stretching, the force decays and the decay rate is progressively reduced. After 5 min, the force does not decrease more than within 5% in the following 5 min. Although no real plateau is observed in a log(force)−log(time) representation, this small decay leads to the assumption that the samples are close to equilibrium under tension. This equilibrium force, f_{eq}, has been used to calculate the reduced stress, G[16-22]

$$G = \frac{f_{eq}}{l_f e_f \left(\lambda^2 - \frac{1}{\lambda}\right)} \quad (1)$$

where l_f and e_f are the width and the thickness of the sample after stretching.

Small-Angle Neutron Scattering. The quenched samples were examined using the small-angle neutron scattering technique.[23] θ is defined as the angle between the incident beam and the scattered beam recorded in a given cell of the

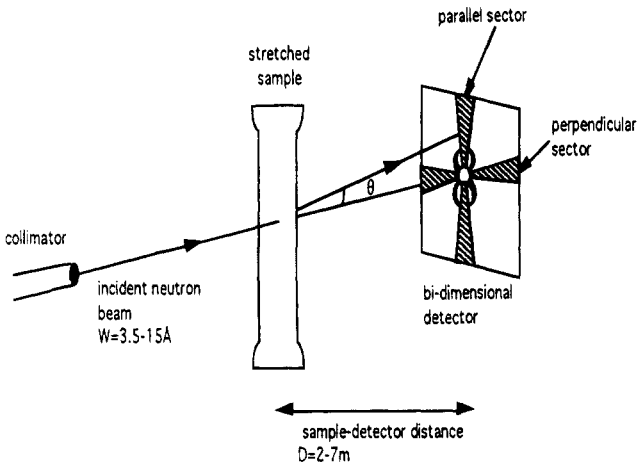

Figure 1. Schematic representation of the neutron scattering experiment.

multidetector. The latter, similar to the X,Y grid of a video camera, is in a plane perpendicular to the incident neutron beam at a distance 3.20 m behind the sample. The wavelength, W, is generally equal to 10 Å. The sample is aligned perpendicular to the incident beam. The scattering vector, **q**, for each detector cell is defined as the difference between the incident wavevector and the scattered wavevector, which form an angle θ. Its modulus is

$$q = \frac{4\pi}{W}\sin\left(\frac{\theta}{2}\right) \tag{2}$$

q will always be in a plane perpendicular to the incident wavevector, which also contains the stretching axis of the sample. However, **q** may have any direction with respect to this axis, indexed by an angle ψ. Important directions are the parallel direction ($\psi = 0°$) and the perpendicular direction ($\psi = 90°$)[24,25] (see Figure 1). The scattering vector range in our configuration is 7×10^{-3} to 7×10^{-2} Å^{-1}. For a given X,Y spectrum, lines may be drawn joining all cells of equal neutron count, called isointensity lines, or one can make a radial averaging of the cells within angular sectors of angle ψ and width $\delta\psi$ ($\delta\psi = 20°$ along the parallel direction and $\delta\psi = 15°$ along the perpendicular direction). The radially averaged spectrum of each sample for one direction is corrected by the radially averaged spectra of pure hydrogenated polystyrene (H-PS), water, and empty cell spectra in the same direction to eliminate the incoherent background, correct for the detector efficiency, and calibrate the results in absolute units (cm^{-1}) denoted $I(q)$ ($I(q)$ is actually a scattering cross-section per unit volume of sample). $I_\psi(q)$ is defined as the corrected spectral intensity along the direction ψ, $I_\perp(q) = I_{\psi=90}(q)$, and $I_\parallel(q) = I_{\psi=0}(q)$.

The dimensionless theoretical scattering, $S(q)$, is defined as

$$I(q) = \left(\frac{a_H}{v_H} - \frac{a_D}{v_D}\right)^2 vS(q) \tag{3}$$

where $v_H = v_D = v$ is the volume of the monomer, normal or deuterated, and a_H and a_D are their total scattering lengths.

3. Results

3.1. Isotropic Samples. Effect of the Cross-Linking Density. Consider first the two samples, AR143 and AR153, with the same value $M_{WD} = 73\,000$ and a different cross-linking density characterized by an increasing aminomethylation rate $1/A$ (1/48 and 1/30, respectively) and a decreasing equilibrium swelling ratio, Q_{eq} (12.7 and 8.6). The two isotropic signals are shown in Figure 2a. The scattering increases with increasing cross-linking ratio.[2] The same effect can be seen in Figure 2b, corresponding to different samples

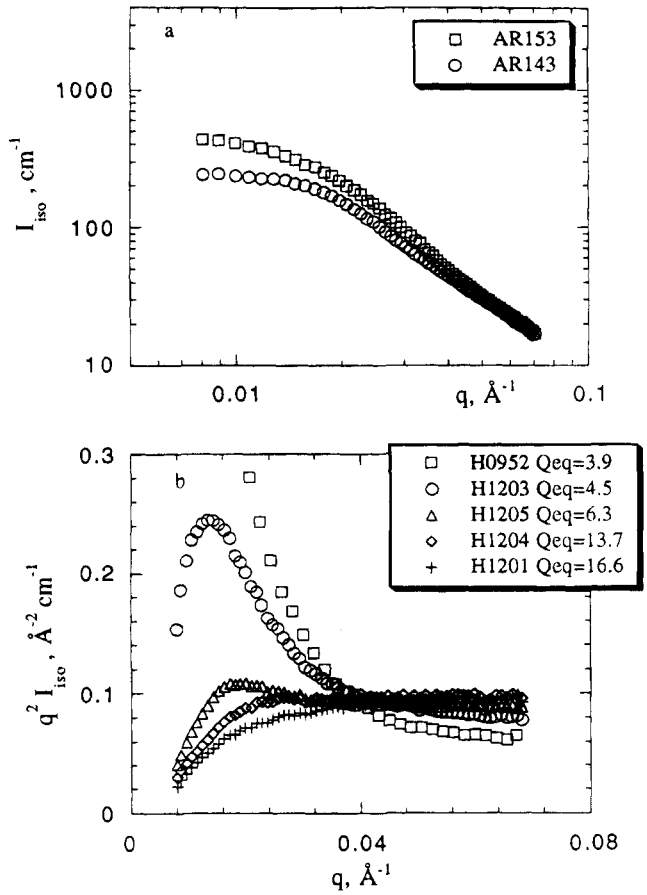

Figure 2. (a) Isotropic scattering, in log–log representation, for two samples of different cross-linking ratio containing large free chains ($M_{WD} = 73\,000$). (b) Isotropic scattering (Kratky–Porod representation) for trapped chains ($M_{WD} = 138\,000$) in five different samples of increasing cross-linking ratio (decreasing Q_{eq}).

of increasing cross-linking ratio, with the same $M_{WD} = 138\,000$. Here also the signal increases continuously with the cross-linking ratio. The differences are visible at small q, while at large q, $S(q) \sim 1/q^2$; that is, $q^2S(q)$ is close to a plateau for the cross-linked samples as well as for a polymer mixture (melt) made of these two types of chains. In the latter case, it was checked earlier that the form factor of a single chain was that of a Gaussian chain and that deuterated and hydrogenated polystyrene are mixed at random. More precisely, we consider the equation[26]

$$\frac{1}{S(q)} = \frac{1}{\phi_H S_{1H}(q)} + \frac{1}{\phi_D S_{1D}(q)} - 2\chi_{HD} \tag{4}$$

often called the RPA equation, with the interaction parameter, χ_{HD}, very close to 0 (2×10^{-4}) here[27] and $S_{1H}(q) = N_H P_H(q)$, where $P_H(q)$ is the form factor, given in the case of Gaussian chains by the so-called Debye function:

$$P_H(q) = 2\left(\frac{e^{-x} - 1 + x}{x^2}\right) \tag{5}$$

where $x = q^2R_{gH}^2$, and N_H is the number of monomers in the chain. Similar definitions hold for $S_{1D}(q)$.

Equation 4 is used to compute the scattering from an un-cross-linked mixture of deuterated and nondeuterated chains of the same molecular weight as the one used to synthesize the networks with trapped chains.

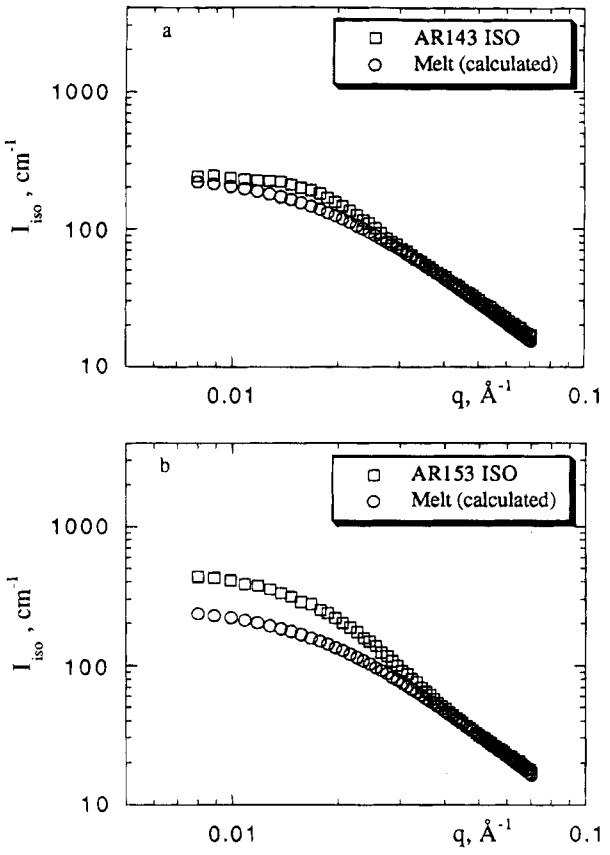

Figure 3. Comparison, in log–log representation, between isotropic scattering from cross-linked samples containing free chains (M_{WD} = 73 000) and the computed signal of an un-cross-linked mixture: (a) AR143; (b) AR153.

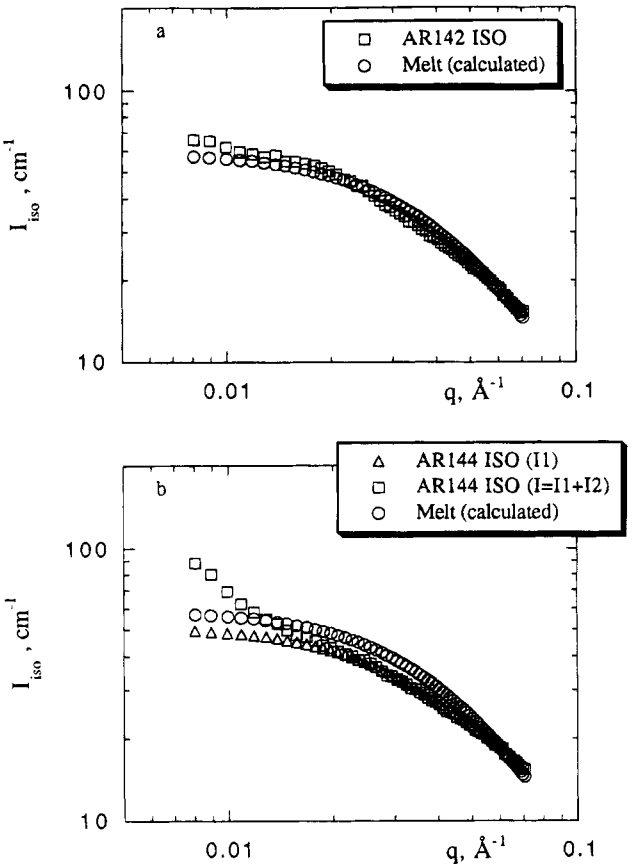

Figure 4. Comparison, in log–log representation, between the isotropic scattering from cross-linked samples containing free chains (M_{WD} = 73 000) and the computed signal from an un-cross-linked mixture: (a) AR142; (b) AR144 [(□) measured signal I; (△) corrected signal $I_1(q) = I(q) - I_2(q)$ after subtraction of a Debye–Bueche contribution; (○) computed signal of an un-cross-linked mixture].

The front factor for this computed signal is estimated using the value of the plateau of $q^2S(q)$ at large q. Comparison with the corresponding network data, Figure 3a,b, shows an increase in the intensity, $I(q)$, at small q with increasing cross-linking ratio.

The same trends are also observed for the other molecular weights studied here, M_{WD} = 14 370, in Figure 4a,b, for the two samples AR142 and AR144. The measured values are greater than the computed values for the random mixture at low q and slightly lower at intermediate q. For larger trapped molecular weights, M_{WD} = 138 000 and M_{WD} = 751 000,[2] the effect of the cross-linking density is similar.

Effect of the Molecular Weight. Figure 5 compares the intensity profiles of samples of equivalent cross-linking ratios but different molecular weights: The scattering increases when M_{WD} passes from 14 370 (AR142) to 73 000 (AR143) as seen in Figure 5a as well as from 138 000 (H1201) to 751 000 (H0601) (Figure 5b). This is also true for the small chains (14 370) included by posttrapping (dipping) compared to the long chains (73 000) included by cotrapping.

Data Analysis. In section 4 it is explained that the classical models do not predict an increase at $q \to 0$ for a random mixture as given by eq 4 with $\chi = 0$. We therefore attempt to describe the signal as an interchain one, observed here by a comparison with a Lorentzian function

$$I(q) = \frac{I_0}{1 + q^2\xi^2} \tag{6}$$

A variation of ξ can be obtained, for example, from eqs 3 and 4 at low q with $\chi > 0$, using $1/S_D(q) = [1/S_D(q\to 0)](1 + q^2R_{gD}^2/3)$, and the same for $S_H(q)$. The apparent ξ is a combination of the radii R_{gH}, and R_{gD} for $\chi = 0$ but increases with $\chi > 0$.

Adjusting the signal to a Lorentzian form is delicate: A first difficulty is when, for example in Figure 4b, an upturn is observed at $q \to 0$ since a true Lorentzian profile would yield a plateau. The signal is fitted to a sum

$$I(q) = I_1(q) + I_2(q) = \frac{I_{01}}{1 + q^2\xi^2} + \frac{I_{02}}{(1 + q^2\Xi^2)^2} \tag{7}$$

where $I_1(q)$ is drawn in Figure 4b and $I_2(q)$ is a Debye–Bueche law, representing scattering from large heterogeneities with flat interfaces. Such heterogeneities were attributed earlier to some kinds of ionomer clusters of aminomethylated groups in these networks.[2] It is noted here that $I_2(q)$ is important only for the sample corresponding to Figure 4b (AR144), for which $I_1(q)$ is inferior to the calculated scattering for a random mixture. For other samples we could just ignore the first points for a fit with $I_1(q)$ only.

Another difficulty is, however, encountered at intermediate q: at variance with eq 4, the slope is higher than −2, which leads to a curvature in the usual $1/I(q)$ vs q^2 representation used to extrapolate ξ.

The fit to eq 4 gives the values of I_0 and ξ of Table 3. Both quantities increase with the cross-linking ratio.

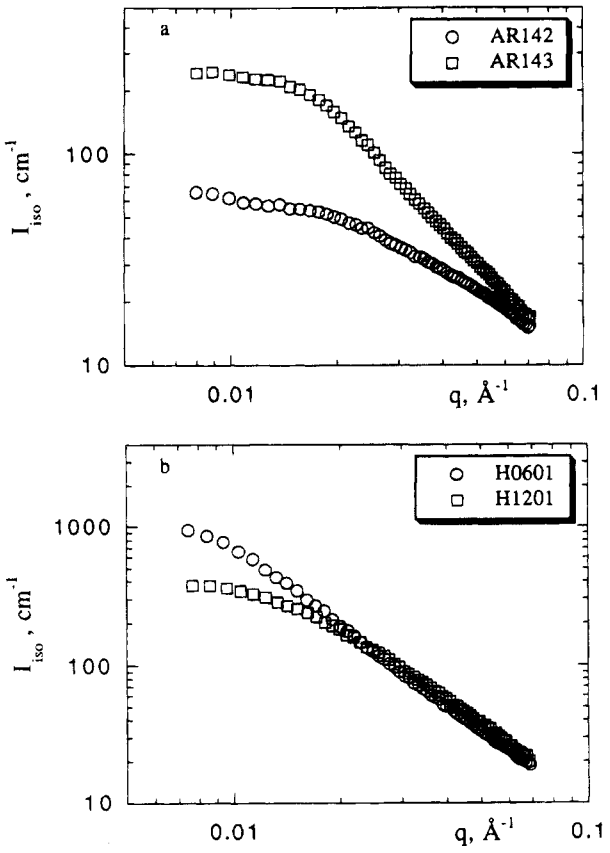

Figure 5. log–log plot of the scattering from the trapped chains in isotropic networks prepared with the same precursor: effect of the molecular weight (see Table 2).

Table 3. Scattering at $q \to 0$ ($I_{0\parallel}$) and Correlation Length ($\xi_\parallel$) in the Parallel Direction for Representative Samples Studied at Different Elongation Ratios, λ

sample	elongation ratio λ	signal $I(q)^a$		signal $I(q)/S_1(q)^b$	
		$I_{0\parallel}$ (cm^{-1})	$\xi_\parallel$ (Å)	$I_{0\parallel}$ (cm^{-1})	$\xi_\parallel$ (Å)
AR143	1	273.22	38.76	1.72	26.80
	1.2	487.80	59.26	3.39	57.66
	1.4	1050.4	97.82	6.10	87.65
	1.6	1605.1	110.30	11.11	124.28
	1.8	2451.0	133.76	16.69	157.19
	2	3311.2	151.00	18.69	168
	2.1	4830.9	182.31	22.27	193.43
	2.25	6369.4	223.32	31.15	228.77
AR142	1	65.22	28.05	1.28	17.26
	1.2	72.74	33.85	1.37	20.66
AR144	1	51.55	24.35	1.01	8.66
	1.2	64.10	30.06	1.23	16.02
	1.3	68.49	32.48	1.32	19.82
	1.4	75.76	35.89	1.46	23.87
	1.6	96.15	44.51	1.80	32.10
	1.8	107.3	49.02	2.04	37.97
	2	121.5	54.34	2.30	42
AR153	1	632.91	71.16	2.3	29.4
	1.2	1459.9	106.64	4.1	47.74
	1.3	2314.8	130.08	5.5	56.06
	1.45	4694.8	183.98	7.87	71.92
	1.6	6993	215	11.38	90.5
	1.85	20080	371	15.36	113.6
	2	36101	514	21.93	141

[a] Experimental signal ($I(q)$). [b] Experimental signal divided by the calculated intrachain form factor ($I(q)/S_1(q)$).

Such a behavior was observed before in similar systems[2] and also by other authors,[28,29] which will be discussed below.

Kinetics. It is known from former measurements[2] that the butterfly patterns appear after a relaxation time, t_R, of the order of the terminal time of a melt made of the corresponding free chains. It was inferred from this that the chains have to be in an isotropic state in order to produce the maximum of the effect. It was checked in one case (by extrapolation from measurements at variable ϕ_D), for $M_{WD} = 34\,000$, that the single-chain form function was isotropic and equal to that of a Gaussian chain. Nevertheless, the relaxation of the network itself should play a role.

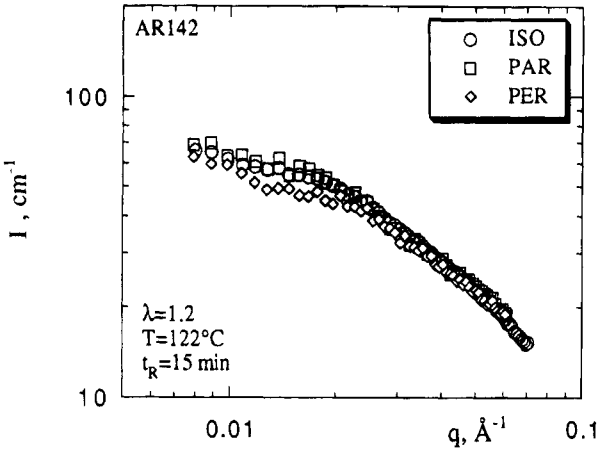

Figure 6. log–log plot of the scattering in the parallel (□) and perpendicular directions (◇) for sample AR142 for an elongation ratio $\lambda = 1.2$ after a relaxation time of 15 min at 122 °C compared to the scattering of the isotropic state (○).

The kinetics of the signal from a deformed network containing some small chains has been studied. The terminal time of the latter is expected to be smaller than the largest relaxation time of the network. The effect of the relaxation of the network is thus expected to be observed. In practice, $M_{WD} = 14\,370$, and the sample has been stretched at a temperature very close to T_g in order to reach very short times. Instead of increasing the relaxation duration, the same time has been used, but at increasing temperature, using the WLF time–temperature superposition principle. The elongation ratio was rather low, $\lambda = 1.2$. By decreasing the temperature to $T = 94$ °C[30] and with $t_R = 5$–15 min, quasi-circular isointensities, or elliptical shapes of very low anisotropy, without the butterfly effect, were observed. This t_R is an estimate of the terminal time at this temperature. On increasing the temperature, butterfly patterns appear after a relaxation of 15 min at $T = 96$ °C, which corresponds to an increase in t_R by a factor of 3. $I(q)$ was measured at temperatures up to $T = 122$ °C (Figure 6), which corresponds to a total increase of t_R by a factor

$$\frac{t_{ter}(T = 122°C)}{t_{ter}(T = 94°C)} = \frac{10^{\frac{13.7(122-90)}{50+122-90}}}{10^{\frac{13.7(94-90)}{50+94-90}}} \approx 21455$$

Over this wide time range, the scattering in the parallel direction, readily large enough to give rise to butterflies at 96 °C, is only increased by 20%. Simultaneously, the tensile force is constant. It may be concluded that no slow rearrangements have any important effect for this elongation ratio, neither on the force nor on the butterfly patterns which appear very suddenly. In this experiment, the relevant relaxation of the network is as fast as that of the small chains. It would be interesting to study the case of a network much less cross-linked, which would have a larger relaxation time and also larger deformations.

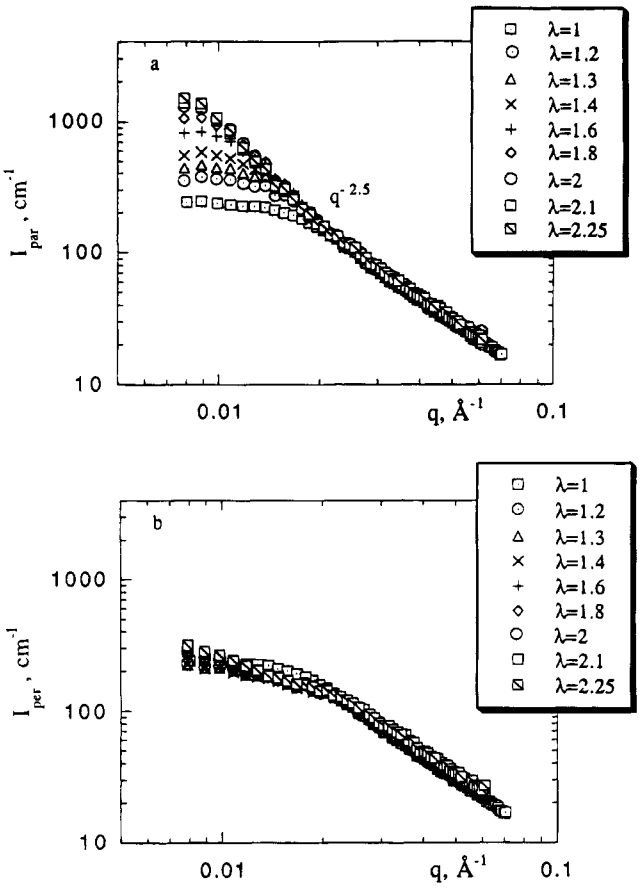

Figure 7. Scattering, in a log–log representation, in the parallel (a) and perpendicular (b) directions for sample AR143 after a relaxation time of 10 min at 134 °C as a function of the elongation ratio, λ.

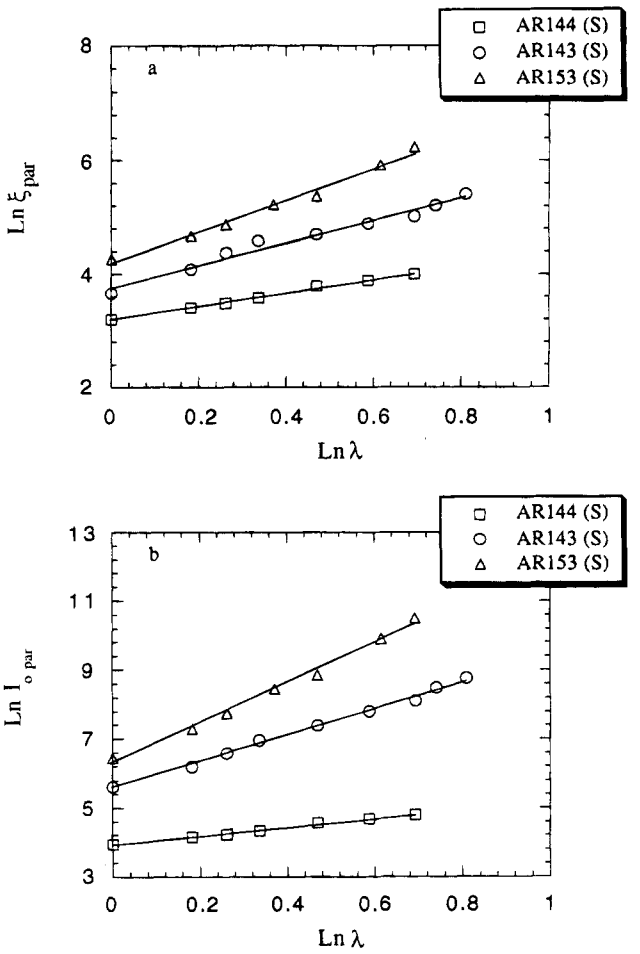

Figure 8. Variation of the correlation length $\xi_{\parallel}$ (a) and the scattering at $q \to 0$, $I_{0\parallel}$ (b), in the parallel direction with the elongation ratio λ for signal $I(q)$ for different samples: (□) AR144; (○) AR143; (△) AR153.

3.2. Effect of the Elongation Ratio: "The Limit Curve". Variation of I(q) in the Parallel and Perpendicular Directions. In the following section, we will consider only samples stretched and subsequently relaxed for a long time (10 min) after a uniaxial stretching at a high temperature (134 °C). Such conditions, following the earlier observations, should correspond to a stable regime. Some of these results were presented before.[31]

Typical intensity profiles are shown in Figure 7 for $M_{WD} = 73\,000$ and $A = 48$ (AR143). At low q, the signal increases along the elongation direction, $I(q_{\parallel})$, with λ, whereas the scattering in the perpendicular direction, $I(q_{\perp})$, decreases to the scattering of an ideal mixture and stabilizes for $\lambda > 1.2$. In the parallel direction, the intensity as a function of q in a log–log plot can be divided into three regions: a plateau at low q, which transforms at $q \sim q_p$ into a quasi-linear decrease at larger q and connects finally with a second linear decrease of slope -2 ($I(q) \sim q^{-2}$). When the deformation ratio, λ, is increased, the plateau region increases in height, the value of q_p is shifted toward lower q's, and in the central region, the curves collapse progressively to a pseudo *limit curve*, which can be approximated by a power law $I(q) \sim q^{-2.5}$. In the perpendicular direction, the variation with λ at low q is different. In the central region of the q range, $I(q_{\perp})$ decreases slightly compared to $I_{iso}(q)$ when passing from $\lambda = 1-1.2$, and then remains essentially identical at larger λ and overlaps the calculated signal for ideal mixing. In the lowest q range, however, in contrast with $I_{iso}(q)$, which is flat at low q, $I_{\perp}(q \to 0)$ displays a slight upturn, visible when λ reaches 1.8 and progressively increasing up to $\lambda = 2.25$. Equation 7 could account for this, if (i) $I_1(q_{\perp})$ first decreases, compared to I_{1iso}, and then stabilizes or (ii) $I_2(q_{\perp})$ increases slowly compared to I_{2iso}.

On the contrary, in the parallel direction, no upturn is observed: I_2 may have decreased or simply become negligible compared to the strong increase of I_1.

The upturn in the perpendicular direction could also be due to a radial average in a too-wide angular sector. Let us define ψ^* by $\lambda^2 \cos^2 \psi^* + 1/\lambda \sin^2 \psi^* = 1$, the angle at which the effective deformation ratio is 1 (see below). For $\psi^* < \psi < 90°$, the deformation corresponds to a contraction. The problem is that ψ^* varies from 55° (its limit at $\lambda \to 1$) to 70° for the largest $\lambda = 2.25$. In principle, by regrouping on a sector $\psi = 90 \pm 15°$, ψ remains greater than ψ^* but involves deformation different from the pure perpendicular one. At a smaller angle, due to resolution effects, we may involve direction $\psi < \psi^*$ for which $\lambda_{eff} > 1$. Thus it would be useful to check these effects with narrower sectors and at lower resolution.

I_0 and ξ may be extracted (eq 6) in the range where $1/I(q)$ is linear with q^2 in the range $q < q^* = 1/\xi$. In the perpendicular direction, the upturn of $I(q_{\perp})$ at low q is ignored, but the upper part of the range $q < q^*$ is still available, which, together with a normal crossover to q^{-2} at $q > q^*$, allows for a good fit. In the parallel direction, the absence of an upturn makes the fit easier, but at large λ, q^* becomes too low, or even vanishes ($q^* \leq q_{min}$). The $q^{-2.5}$ behavior at $q > q^*$ also makes the fit more delicate at large q (since it differs from the q^{-2}

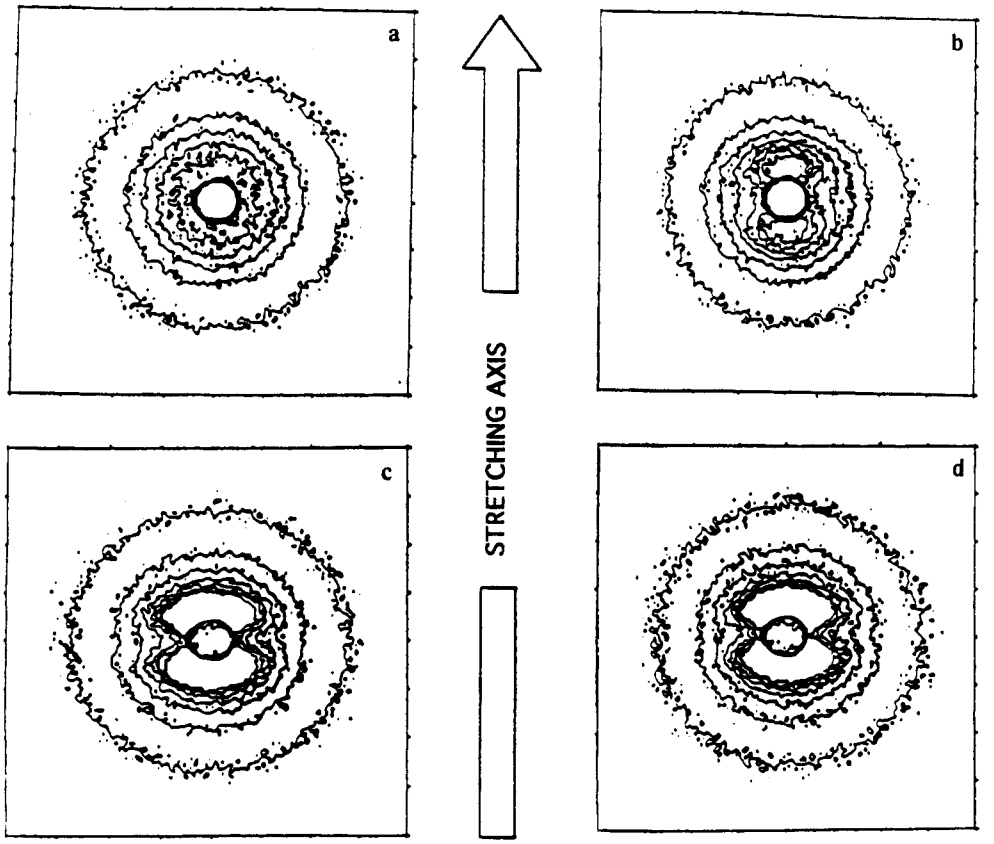

Figure 9. Isointensity patterns for sample AR143 after a relaxation time of 10 min at 134 °C for different values of the elongation ratio: (a) $\lambda = 1$; (b) $\lambda = 1.2$; (c) $\lambda = 2$; (d) $\lambda = 2.25$.

behavior of eq 6 at $q > 1/\xi$). The apparent values of I_0 and ξ are given in Table 3 and the variation of $\ln(I_0)$ (respectively $\ln(\xi)$) with $\ln(\lambda)$ is plotted in Figure 8: it is linear with a slope of 3.84 (respectively 1.98) for sample AR143.

At the largest q's, the variation of $I(q)$ is again close to q^{-2}, as in the isotropic state as seen in Figure 7. However, plots more sensitive at large q ($q^2I(q)$ vs q) show that $I(q_{\parallel})$ decreases and $I(q_{\perp})$ increases with increasing λ, following the prediction of the classical models of elasticity (see discussion).

The effects described above for $I(q_{\parallel})$ and $I(q_{\perp})$ can also be seen in the isointensity curves (Figure 9). The fact that $I(q_{\parallel})$ increases with λ corresponds to stronger and neater "butterfly patterns". At low q, the patterns are double-winged, looking like eights. When increasing λ, they look inscribed inside an elliptic envelope. The increase in $I(q_{\parallel})$ corresponds to new isointensity lines appearing close to the beam axis. No change in shape is observed between $\lambda = 2$ and 2.25. This corresponds to the overlap of curves in the parallel direction as well as for the majority of the directions, ψ.

Figure 10 shows the variation of $I(q)$ as a function of q at an intermediate angle $\psi = 55°$ (equal to $\psi^*(\lambda=1)$) for different values of λ. The scattering profile resembles very much that for which $\psi = 0°$. For each λ, one can interpolate a value, $\lambda^{app}(\psi)$, for which $I^{\lambda^{app}}(q,\psi=0°) \sim I^{\lambda}(q,\psi=55°)$. The values are given in Table 4 and compared to the values $\lambda^{eff}(\psi)$, where

$$\lambda_{eff}^2(\psi) = \lambda^2 \cos^2 \psi + 1/\lambda \sin^2 \psi \qquad (8)$$

At first sight, the two values are relatively close. Looking more closely, λ^{app} is generally slightly larger than λ^{eff} (i.e., 1.2 rather than 1.127), and this effect decreases with decreasing λ.

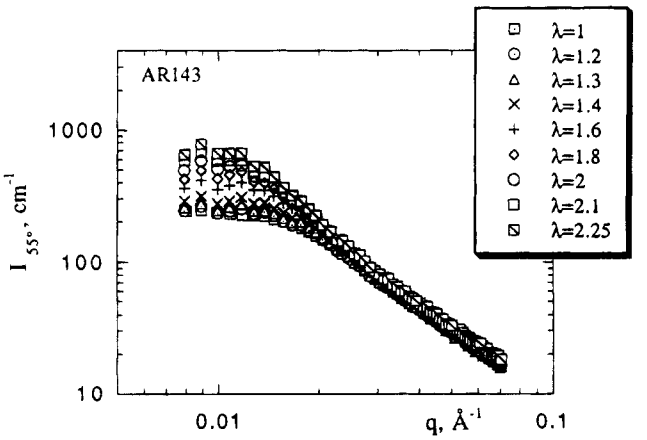

Figure 10. Scattering, in a log–log representation, in the direction $\tilde{\psi} = 55°$ (corresponding to 3 $\cos^2 \tilde{\psi} = 1$) for sample AR143 after a relaxation time of 10 min at 134 °C as a function of the elongation ratio, λ.

Table 4. Values of Effective (λ_{eff}) and Apparent (λ_{app}) Elongation Ratio Relative to the Experimental λ's for Sample AR143

λ	λ_{eff}	λ_{app}
1	1	1
1.2	1.017	1
1.3	1.037	1.05
1.4	1.06	1.1
1.6	1.127	1.2
1.8	1.2	1.25
2	1.225	1.35
2.1	1.337	1.4
2.25	1.4	1.45

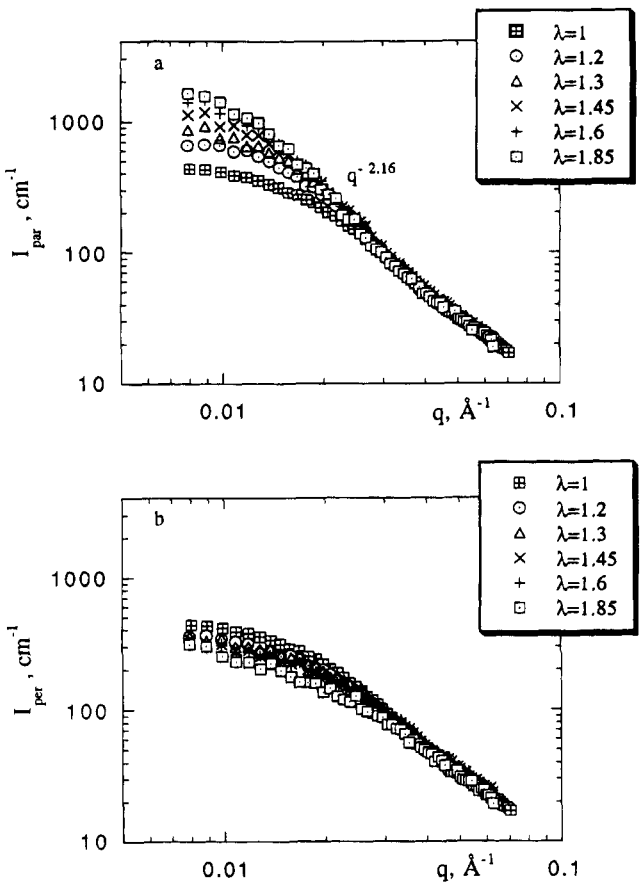

Figure 11. Scattering, in a log–log representation, in the parallel (a) and perpendicular (b) directions for sample AR153 after a relaxation time of 10 min at 134 °C as a function of the elongation ratio, λ.

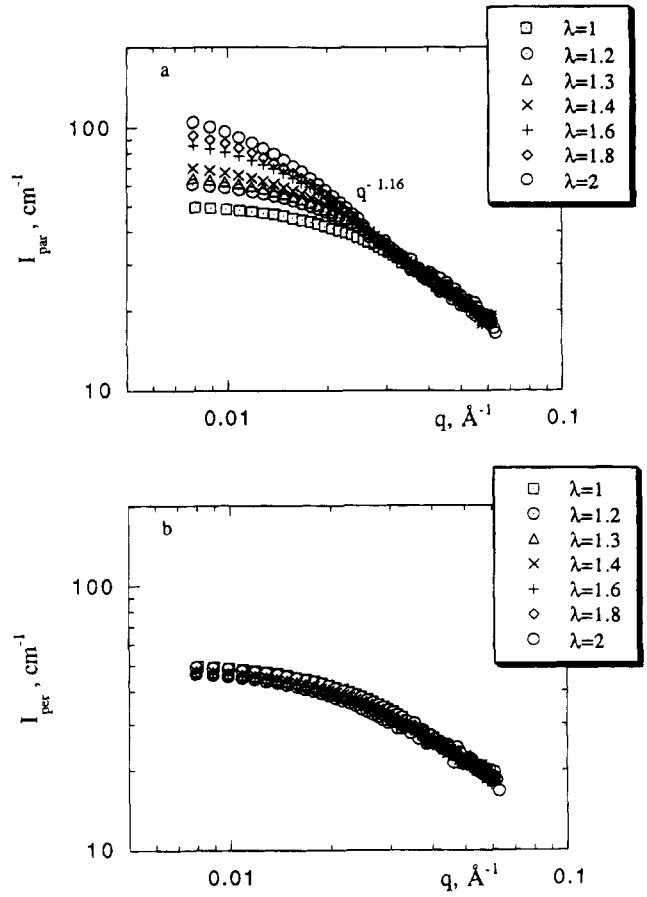

Figure 12. Scattering, in a log–log representation, in the parallel (a) and perpendicular (b) directions for sample AR144 after a relaxation time of 10 min at 134 °C as a function of the elongation ratio, λ.

The effects described above for sample AR143 are relatively similar for sample AR153, which is more cross-linked (Figure 11a,b). The crossover value, q^{**}, below which $I(q_{\parallel})$ departs from classical behavior and increases with λ, is smaller for this higher cross-linking ratio. For both samples, q^{**} is also the value below which $I_{iso}(q)$ departs from the random mixing behavior. $I(q_{\parallel})$ falls again progressively on a limit curve when λ increases; the maximum value is $\lambda = 2$, above which the sample broke. $I(q)$ as a function of q is therefore a straight line for this limit with a slope 2.16. The increase in $I_{\parallel}(q \to 0)$ is higher, for the same λ, then that for the less cross-linked sample, and for any given value of λ (including $\lambda = 1$), $I(q_{\parallel})$ is always larger. In addition, when λ passes from 1 to 1.2, the decrease in $I(q_{\perp})$ is greater than for sample AR143, in association with the higher value in the isotropic state. No apparent $I_2(q)$ contribution is needed here to describe the results. From $\lambda = 1.4$ to $\lambda = 2$ in the medium-q range, $I(q_{\perp})$ decreases progressively back to the ideal mixing, which is reached here only for $\lambda \sim 2$ (ignoring the upturn for the first two points). At large q, $I(q_{\perp}) > I_{iso}(q) > I(q_{\parallel})$, with a stronger anisotropy than for AR143, in agreement with the classical models. Values of I_0 and ξ (Table 3), are larger, and their variation with λ is characterized by a stronger exponent (Figure 8a,b).

Effect of the Molecular Weight of the Trapped Chains. For the smaller molecular weight, $M_{WD} = 14\,370$, a higher contribution of $I_2(q)$ at low q as seen in the isotropic state already is observed as well as a lower variation of the main contribution $I_1(q)$ with λ. The $I_2(q_{\perp})$ term increases, as above, but more markedly, with increasing λ, and its range is shifted toward larger q, as expected for an affine deformation. Similarly, $I_2(q_{\parallel})$ is shifted toward lower q values. This is directly visible for sample AR144, for which I_2 is large.

After fitting the data to eq 7, the I_2 contribution is removed. In Figure 12a,b, a clear increase in $I_1(q_{\parallel})$ in the intermediate q range is evident and the vertical shift in log $I(q_{\parallel})$ with respect to log $I_{iso}(q)$ is smaller than for samples AR143 and AR153 when increasing λ. It is difficult, however, to distinguish a limit curve, and even more to assign a slope to it. An apparent value is of the order of 1.13 ± 0.2, that is, much smaller than for samples with larger molecular weights. In the perpendicular direction, $I_1(q_{\perp})$ first decreases and then remains constant for $\lambda = 1.2$–2.

The I_0 and ξ values extracted from the data are reported in Table 3. One can extract I_0 and ξ from $I(q)/S_1(q)$, where $S_1(q)$ is the form factor of a Gaussian chain (as used in eq 4). The values are given in the same table and plotted in Figure 13. The exponents, from fits of their variation with the elongation ratio λ, are listed in Table 5 for different samples.

Mechanical Measurements. Figure 14 shows the value of the apparent modulus, G (also called the reduced stress), as a function of $1/\lambda$ for the different samples: AR143, AR153, AR144, and AR141 (same precursor as AR143 and AR144, but prepared without trapped chains). Comparison of the plots for AR141, AR144, and AR143, which have the same aminomethylation rate, $1/A = 1/48$, suggests that these measurements should be checked for other samples since the results suggest that the cotrapping of longer chains reduces the modulus. Longer chains may reduce the

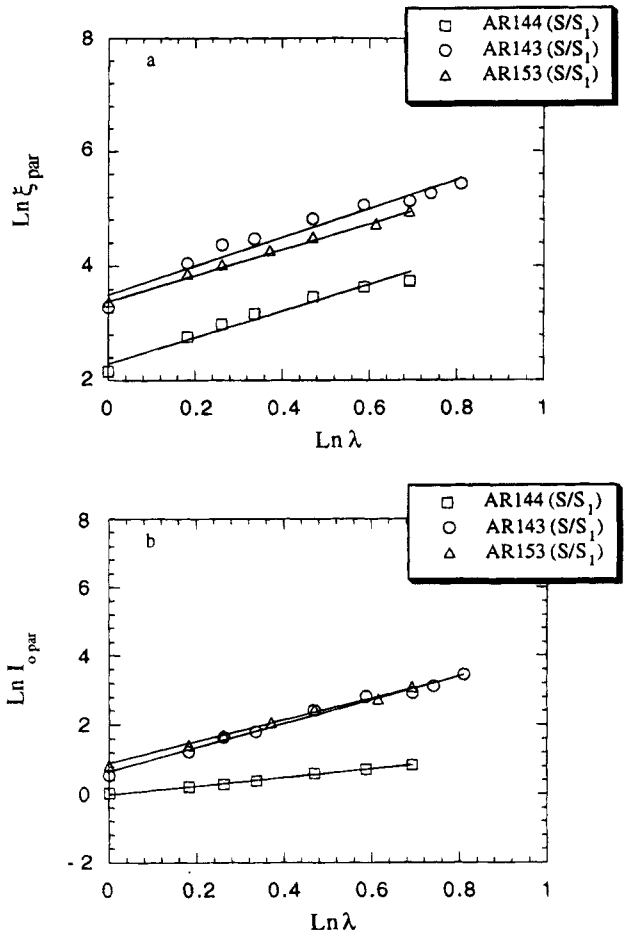

Figure 13. Variation of the correlation length $\xi_{\parallel}$ (a) and the scattering at $q \to 0$, $I_{0\parallel}$ (b), in the parallel direction with the elongation ratio λ for signal $I(q)/S_1(q)$ for different samples: (□) AR144; (○) AR143; (△) AR153. ($S_1(q)$ is the intrachain form factor.)

Table 5. Apparent Exponents for the Power Law Variation of the Scattering at $q \to 0$ ($I_{0\parallel}$) and the Correlation Length ($\xi_{\parallel}$) with the Elongation Ratio λ for Signals $I(q)$ and $I(q)/S_1(q)$

	signal $I(q)$		signal $I(q)/S_1(q)$	
sample	$I_{0\parallel}$	$\xi_{\parallel}$	$I_{0\parallel}$	$\xi_{\parallel}$
AR143	3.84	1.98	3.46	2.40
AR144	1.27	1.2	1.2	2.26
AR153	5.84	2.82	3.2	2.2

number of contacts for cross-linking, either because of their larger size or because of the larger object created by a beginning separation between free chains and clusters of H-chains during network formation.

For the same M_{WD}, sample AR153, which corresponds to a higher aminomethylation rate ($1/A = 1/30$, rather than 1/48), displays higher modulus values. The plots (Figure 14) G *versus* $1/\lambda$, called Mooney–Rivlin representations, display a decay of G when $1/\lambda$ decreases from 1 ($\lambda = 1$) to 0 ($\lambda = \infty$), i.e., a "shear-thinning" behavior, often observed for networks in the bulk state. The Mooney–Rivlin formula is written as[32-35]

$$G = 2C_1 + \frac{2C_2}{\lambda} \qquad (9)$$

The values of $2C_1$, $2C_2$ and $2C_1 + 2C_2$ derived from Figure 14 are listed in Table 6. The values of λ_{break}, corresponding to the elongation ratio at which the sample broke within less than 10 min, are also listed

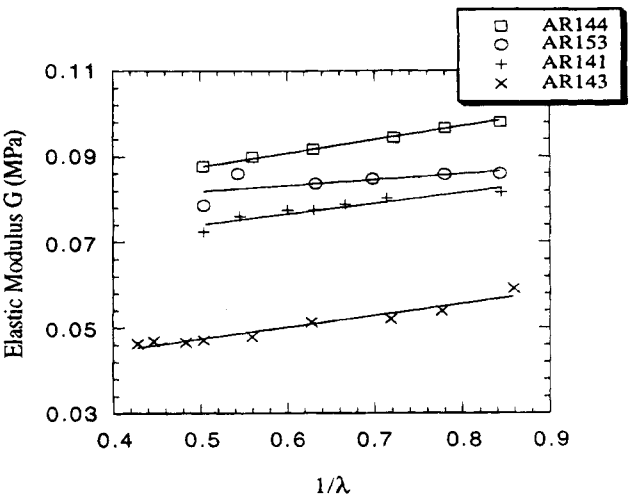

Figure 14. Mooney–Rivlin representation of the apparent elastic modulus, G, as a function of the inverse of the elongation ratio λ^{-1}, the constants leading to $2C_1$ and $2C_2$, for different samples.

Table 6. Values of $2C_1$, $2C_2$, and $2C_1 + 2C_2$ Obtained from the Mooney–Rivlin Representation (eq 9), Elongation Ratio at Rupture (λ_{break}), and the Relaxation Time after Stretching t_R

sample	$2C_1$ (MPa)	$2C_2$ (MPa)	$(2C_1 + 2C_2)$ (MPa)	λ_{break}	relaxation time t_R (min)
AR141	0.062	0.025	0.087	2	15
AR143	0.034	0.027	0.061	2.35	10
AR144	0.072	0.030	0.102	2	10
AR153	0.075	0.014	0.089	2	10

in the same table. λ_{break} is higher when the modulus is noticeably lower.

4. Discussion and Comparison with Some Theoretical Models

We will discuss and compare the results with various theoretical predictions. We consider first models issued from linear elasticity theory.

4.1. Effect of Chain Deformation in Basic RPA.

In the classical theories of chain deformation in networks, because of the cross-linking, a part of the external deformation is transmitted down to short length scales, comparable with the size of the mesh (made of N_c monomers). Following these theories, deformation models[18,19,36-39] allow the calculation of $S_2^{\lambda}(q)$, the form factor of chains fixed to the network, as a function of λ and N_c. Using the simple RPA eq 4, we could replace the scattering of the free chains, $S_{1D}(q)$, or of the network chains, $S_{1H}(q)$, by their values under deformation. The latter are linked together with the interchain scattering by incompressibility.

The un-cross-linked labeled chains are able to rearrange, letting $S_{1D}^{\lambda}(q)$ essentially undeformed, as checked earlier. The form factor, $S_{1D}^{\lambda}(q)$, of the free chains in a network was also directly measured.[2] The samples were networks containing a total fraction, ϕ_T, of free chains, but only a part of them, representing a fraction ϕ_D, was deuterated. ϕ_D was varied at constant ϕ_T, allowing extrapolation at zero ϕ_D for extracting the form factor (that is, the intrachain correlations). We found S_{1D} isotropic; the free chains had recovered their isotropic Gaussian configuration both after drying and after stretching at large t_R.

Only $S_{1H}^{\lambda}(q)$ is noticeably modified by the deformation, as directly measured in a earlier publication:[40] the samples consisted of a fraction, ϕ_D, of deuterated chains

cross-linked together with nondeuterated chains of the same molecular weight. We found that they were deformed, *qualitatively*, as predicted by the classical models of elasticity.

We can now predict the result of eq 4. For isotropic samples the only deformation is deswelling during drying, i.e., a compression by a factor $\lambda = (10.54)^{-1/3} = 0.456$. Crudely speaking, the linear density is increased by the compression; therefore $S_{1H}{}^{\lambda}(q)$ becomes higher. The cross-linking density is probably lower during this step than its value after the final step of heating in the nearly dry state. However, in eq 4 the contribution of $1/S_{1H}{}^{\lambda}(q)$ is weighted by $1/\phi_H \approx 1.25$. This value is small compared to $1/\phi_D \approx 5$ and privileges the contribution of $1/S_{1D}{}^{\lambda}(q)$. No change should be seen at $q \to 0$ since $S_{1H}{}^{\lambda}(q \to 0)$ remains equal to the molecular weight for any deformation.

Effect of the Molecular Weight. We compare now, for a given precursor and for approximately the same cross-linking density, the signal for $M_{WD} = 73\,000$ to that for $M_{WD} = 14\,370$. The former scattered signal is clearly greater; this is actually also observed for an ideal mixture. It seems therefore more sensible to compare the signal, $S(q)$, scattered from each network to that from an ideal mixture, or to the form factor, $S_{1D}(q)$. We observe in Table 3 that the zero-q limit of $S(q)/S_{1D}(q)$ is 1.72 for $M_{WD} = 73\,000$ and 1.28 for $M_{WD} = 14\,370$ for the same precursor $A = 48$. Thus, for this pair of samples, the enhancement of scattering is larger than the increase due to $S_{1D}(q)$ (proportional to the molecular weight). This may be due either to the structure of the network depending on the molecular weight of the trapped chains or to a more heterogeneous distribution of the free chains in the case of the larger molecular weight. However, this effect is not observed for the pairs of samples plotted in Figure 5a,b. In such cases, the ratio of the zero-q limit of the two signals is *lower* than the ratio of the masses.

Effect of the Stretching. In the stretched case, $S_{1H}{}^{\lambda}(q)$, measured directly, is larger in the perpendicular direction than in the parallel direction, and the same for the scattering at $q \to 0$ for any direction ψ. Isointensities are ellipses, sometimes lozenges, always with the great axis perpendicular to the stretching axis. Using eq 4, $S(q)$ should also be larger in the perpendicular direction than in the parallel direction and at $q \to 0$, intensities in the principal directions should merge. The isointensity lines should be ellipses of major axis perpendicular to the stretching axis, with a rather smaller anisotropy at large q, since $S(q)$ is dominated by the signal from the free chains. Clearly, this is not observed. We have to look for some other types of correlations.

4.2. Linear Elasticity Theory: Homogeneous and Heterogeneous Cases. We now consider the simplest predictions from classical elasticity as put in the most precise form by Onuki. The starting point is the free energy (bilinear terms only),[13,17,26,41] which after Fourier transform and using the fluctuation dissipation theorem gives for a gel swollen (concentration ϕ) and stretched (elongation ratio λ)

$$S_{\text{therm}}^{\text{gel}}(q) \approx \frac{k_B T}{a^3} \frac{\phi^2}{K_{\text{gel}}^{\text{osm}} + \frac{1}{3}\mu + \mu J(\psi) + M(\psi) q^2} \tag{10}$$

where

$$J(\psi) = \lambda^2 \cos^2 \psi + 1/\lambda \sin^2 \psi \tag{11}$$

$$M(\psi) = MJ(\psi)$$

$$\mu = v_0 k_B T \left(\frac{\phi}{\phi_0}\right)^{1/3} \tag{12}$$

The first term in the denominator corresponds to the first term in the free energy (eq A-2 in the Appendix), i.e., the energy of mixing, which itself contains an elastic energy of swelling (eq A-2), so that

$$K_{\text{osm}}^{\text{gel}} = K_{\text{osm}}^{\text{sol}} - \frac{\mu}{3} \tag{13}$$

One assumes that the mixing energy is the same in the solution and in the network, in slight disagreement with experiment for gels.[42] Mapping eq 8 to the case of a blend of short chains in cross-linked long chains, one obtains a modification of the RPA (eq 4) in the form

$$S_{\text{therm}}(q) = \left\{\left(\frac{1}{\phi_H N_H} + \frac{1}{\phi_D N_D}\right)^{-1}\left(\frac{1}{\phi_H N_H P_H(q)} + \frac{1}{\phi_D N_D P_D(q)}\right) - 2\chi - \frac{\mu^*}{3} + \frac{\mu^*}{3} + \mu^* J(\psi)\right\}^{-1} \tag{14}$$

where the form factors, $P_{H,D}(q)$, are given by eq 5, $\chi = \chi_{HD}$ and $\mu^* = \mu v/k_B T$ is a dimensionless modulus ($v \sim a^3$).

If one ignores the last two terms of eq 14, $\mu^*/3 + \mu^* J(\psi)$ (i.e., ignoring $\mu/3 + \mu J(\psi)$ in eq 10 for gels, equal to $4\mu/3$ for the isotropic case), one sees that the scattering increases with cross-linking ratio. This corresponds to the effect of the elastic energy of swelling (eq A-2 in the Appendix), which favors expulsion of the short chains, as argued formerly.[2,28] However, as remarked elsewhere,[13,41,43,44] in principle, the term $\mu^*/3 + \mu^* J(\psi)$ should be present: it represents the effect of the elastic recoil forces, which limits the Brownian motions. In this case the intensity should decrease with increasing cross-linking density. This disagrees qualitatively with our findings (see Figure 3a,b). More quantitatively, let us fit the data to eq 14 for the sample AR143 in the isotropic state. The prefactor between the calculated intensity $I(q)$ and S_{therm}, i.e., $(a_H/v_H - a_D/v_D)^2 v S_{\text{therm}}$, is first determined by fitting to $I_{\text{exp}}(q)$ data at large q, where μ^* is irrelevant. Then, using the measured elastic modulus $2C_1 + 2C_2$, we take $\mu^* = (2C_1 + 2C_2)v/k_B T = 3 \times 10^{-3}$ and $\chi = 0$ (the actual value $\chi_{HD} = 2 \times 10^{-4}$ is negligible). We see that the calculated intensity $I(q)$ is much lower than the data, $I_{\text{iso}}(q)$.

This "classical" treatment of the thermal fluctuations of eq 14 leads also to disagreements under deformation: the term $\mu^* J(\psi)$ leads at low q to a *decrease* in the zero-q limit scattering in the parallel direction. "Butterflies" are obtained, but with *a great axis*, joining the two lobes, *perpendicular to the stretching axis*.

For that reason, Onuki later proposed to supplement eq 14 with a second contribution due to "frozen heterogeneities" fluctuations; because the latter are not correlated with the thermal ones, simple addition is possible. The heterogeneities are considered as a perturbation, $U_{\text{froz}}(r)$. Their response to a deformation—swelling or stretching—could be derived using the fluctuation-dissipation theorem, or by minimization of $\Delta F(q)$

$$\phi_{\text{froz}}(q) = \chi(q) U_{\text{froz}}(q) \tag{15}$$

where

$$\chi(q) = \frac{S_{\text{therm}}^{\text{gel}}(q)}{k_B T} \tag{16}$$

The total scattering is finally

$$S(q) = S_{\text{therm}}(q) + \langle \phi_{\text{froz}}(q)\phi_{\text{froz}}(-q)\rangle = S_{\text{therm}}^{\text{gel}}(q) + \frac{\phi^2}{\alpha^3}\left(\frac{\mu}{\bar{\nu}}\right)^2 \frac{\left[\left(\frac{\phi}{\phi_0}\right)^{2/3} - J(\psi)\right]^2 \langle \nu_0(q)\nu_0(-q)\rangle}{\left\{K_{\text{osm}} + \frac{\mu}{3} + \mu J(\psi) + M(\psi)q^2\right\}^2} \tag{17}$$

$\langle \nu_0(q)\nu_0(-q)\rangle$ is the Fourier transform of the fluctuations in the cross-linking density. Assuming that they are uncorrelated, one has

$$\langle \nu_0(q)\nu_0(-q)\rangle = \bar{\nu}\, p(\phi_0/\phi) \tag{18}$$

where $\bar{\nu}$ is the average cross-link density in the reference state and the dimensionless number p represents the degree of irregularity in the cross-link structure. This entire approach assumes a small perturbation (p small), but the second term may be magnified by the swelling factor ϕ_0/ϕ. For the short chain/network blend

$$\langle \phi_{\text{froz}}(q)\phi_{\text{froz}}(-q)\rangle = p^{**}(\alpha^{-2} - J(\psi))^2 / \left\{\left(\frac{1}{\phi_H N_H} + \frac{1}{\phi_D N_D}\right)^{-1}\left(\frac{1}{\phi_H N_H P_H(q)} + \frac{1}{\phi_D N_D P_D(q)}\right) - 2\chi + \mu^* J(\psi)\right\}^2 \tag{19}$$

In the isotropic state, the added frozen contribution leads now to an increase if $\alpha = (\phi/\phi_0)^{-1/3}$ is not equal to 1. This corresponds to swelling or deswelling, with respect to the preparation conditions, of the heterogeneous structure. The value of α taken for fitting the isotropic state then has to be kept when fitting the deformed state. If the sample is initially "contracted" ($\alpha < 1$), stretching will, in the parallel direction, first compensate this contraction. The calculated signal will first *decrease* before *increasing* again. As this is not observed, we can only take $\alpha > 1$ and assume:

(i) either a small swelling of the network by the short free chains. $\phi_D \sim 20\%$ gives $\alpha^3 = 1.24$. Introducing such a value of α in the fit of $I_{\text{iso}}(q)$ leads to a best fit value of $p^{**} = 0.4$. The signal calculated for $\lambda = 2$ (Figure 15) is then too large by a factor 32! Using the apparent modulus measured for $\lambda = 2$ (lower due to the Mooney–Rivlin effect), μ^* becomes 2.32×10^{-3}; this factor is even larger (36.5).

(ii) or a very large swelling ($\alpha \to \infty$, i.e., $\alpha^{-2} = 0$) which gives the smallest possible $p^{**} = 8.34 \times 10^{-3}$ for fitting I_{iso}. The calculation for $\lambda = 2$ is still far too high.

Reducing $\mu^* - 2\chi$ would reduce this effect. For $\mu^* = 0$ and $\chi = 2.35 \times 10^{-4}$, S_{therm} is sufficient to describe the isotropic sample at all range of $q(\alpha{=}1)$. For $\lambda = 1.6$, a fit is possible with $p^{**}_{\text{fit}}(\lambda{=}1.6) = 20.56 \times 10^{-4}$. However, as seen in Figure 16, (i) the calculated curve is not suitable in shape, strongly above $I_{\text{exp}}(q)$ for intermediate q, and (ii) when λ is increased, one needs to lower p^{**} (i.e., $p^{**}_{\text{fit}}(\lambda_2{=}2) = 9.3 \times 10^{-4}$).

From these two sensible limits of $\mu^* - 2\chi$, it may be concluded that the predictions of uncorrelated frozen fluctuations in eq 17 *are always too strong for* I_0. In addition, the predicted variation of ξ with λ is too weak. The reason for this is that the signal is rapidly dominated by the frozen term, which imposes a constant correlation length.

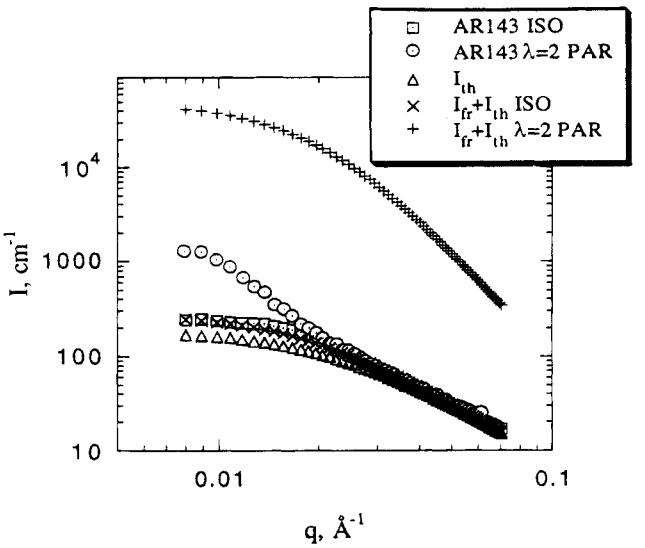

Figure 15. Comparison, in a log–log representation, between the experimental scattering for sample AR143 in the isotropic state and at $\lambda = 2$ and the perturbation model of frozen fluctuations of cross-link density (*cf.* eq 17 and ref 13) corresponding to the same values of the elongation ratio, λ, with the parameters $\alpha^3 = 1.24$, $\mu^* = 3 \times 10^{-3}$, $\chi = 0$, and $p^{**} = 0.4$.

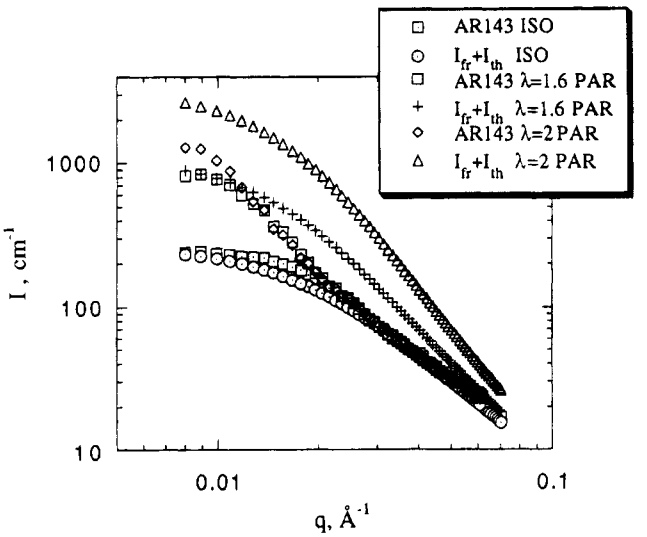

Figure 16. Comparison, in a log–log representation, between the experimental scattering for sample AR143 at $\lambda = 1$, 1.6, and 2 and the perturbation model of frozen fluctuations of cross-link density (*cf.* eq 17 and ref 13) corresponding to the same values of elongation ratio, λ, with the parameters $\alpha^{-2} = 1$, $\mu^* = 0$, $\chi = 2.35 \times 10^{-4}$, and $p^{**} = 20.56 \times 10^{-4}$.

4.3. Enhancement of Spontaneous Fluctuations of Concentration [Rabin–Bruinsma[9]]. This alternative model ignores frozen fluctuation and considers only the thermal term, with an important modification. In eq 14, the thermal term corresponds to simple thermal fluctuations of ϕ and $\vec{u}$ around the free energy minimum for given values of $K_{\text{gel}}^{\text{osm}}$ and μ_{gel}. This corresponds to an affine displacement for $\vec{u}$. Reference 9 introduces for $K_{\text{gel}}^{\text{osm}}$ and μ_{gel} a dependence on ϕ, and, followingly, spatial variations of $K_{\text{gel}}^{\text{osm}}$ and μ_{gel}.

The key point of the calculation is to treat separately the displacement and the polymer concentration and then to couple them using a term C_c div $\vec{u}$ $\delta\phi$. The procedure, still controversial at the moment, gives $\delta\phi$

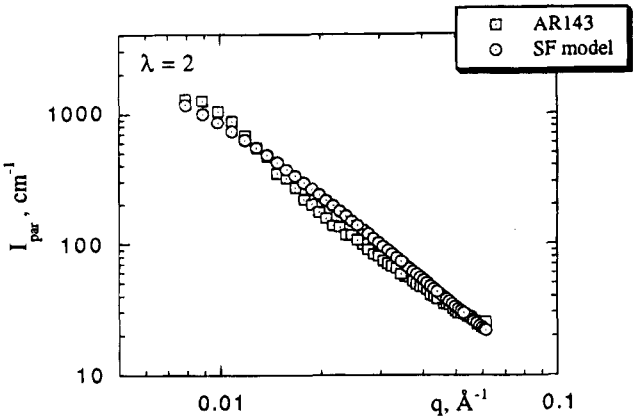

Figure 17. Comparison, in a log–log representation, between the experimental scattering for sample AR143 at $\lambda = 2$ and the model of spontaneous fluctuations (SF) of concentration (*cf.* eq 21 and ref 9) corresponding to the same value of the elongation ratio, λ.

$\cong -\phi$ div $\vec{u}$ for constant moduli. As a result, for the same global deformation, minimizing the energy makes appear more dilute regions which are more deformed, because they are softer, and vice versa. In the system which is initially homogeneous, spontaneous fluctuations appear. The scattering is obtained from the inverse of the free energy given in the q space, $\Delta F(q)$:

$$S(q) \approx \frac{1}{1 + q^2\xi_0^2 - \Gamma(3\cos^2\psi - 1)} \qquad (20)$$

where Γ is proportional to the coupling constant C_c and to the deformation $\lambda - 1$. In models developed for polymer solutions under shear,[10] spontaneous fluctuations enhanced along the flow are also predicted via the dependence of the *viscosity* on the concentration.

As before, we rewrite for the case of the blend

$$S(q) = \left\{\left(\frac{1}{\phi_H N_H} + \frac{1}{\phi_D N_D}\right)^{-1}\left(\frac{1}{\phi_H S_{1H}(q)} + \frac{1}{\phi_D S_{1D}(q)}\right) - 2\chi_{HD} - \Gamma(3\cos^2\psi - 1)\right\}^{-1} \qquad (21)$$

Equation 21 is then equivalent to an "RPA" expression (Lorentzian), as given above (eqs 4 and 6), where Γ $(3\cos^2\psi - 1)$ plays the role of an additional "χ parameter" with a directional dependence. Along the parallel direction, $\Gamma \sim \lambda - 1$ is positive, and the intensity at q tending to zero increases with elongation ratio, λ. In the perpendicular direction, Γ is negative and the scattering decreases.

For the isotropic case, eq 21 can only explain the observed excess scattering of cross-linked systems with respect to an ideal mixture if one assumes a swelling with respect to the preparation state. The latter can be considered as a three-dimensional dilatation.

For the anisotropic state, the model predicts butterfly patterns oriented in the same direction as that observed. We have fitted the data in the *parallel direction* to eq 21. The prefactor between $S(q)$ and $I_{exp}(q)$ is determined at large q as above. Then, for each stretching ratio, we have adjusted $\Gamma_{||}$ in order to fit the experimental zero-q limit, I_{0exp} (see Figure 17 for $\lambda = 2$). The effect of $\Gamma_{||}$ is too strong at intermediate q: $I_{exp}(q) < I_{cal}(q)$ by as much as 40%. This is also related to the fact that the experimental slope in this range of q (2.5 for sample AR143 and 2.2 for sample AR153) is larger than the maximum slope of 2 defined by eq 21. The values of $\Gamma_{||}$ and χ are presented in Table 7.

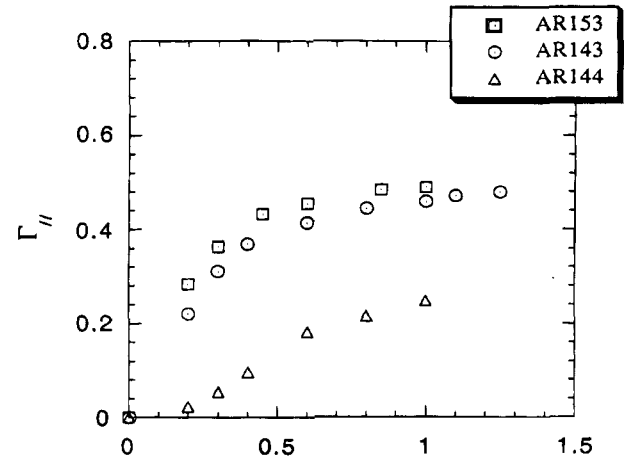

Figure 18. Variation of the parameter $\Gamma_{||}$ extracted from fits of data to eq 21 in the parallel direction with $\lambda - 1$.

Table 7. Values of the Flory–Huggins Interaction Parameter, χ, and the Dimensionless Strain, $\Gamma_{||}$, Extracted from Fits of Data in the Parallel Direction Using Eqs 4 and 21

sample	elongation ratio λ	$\chi \times 10^3$	$\Gamma_{||}$
AR143	1	0.23	0
	1.2	1.96	0.22
	1.3	2.68	0.31
	1.4	3.15	0.37
	1.6	3.50	0.41
	1.8	3.73	0.44
	2	3.84	0.46
	2.1	3.95	0.47
	2.25	4	0.48
AR144	1	1.57	0
	1.2	2.34	0.02
	1.3	3.37	0.05
	1.4	4.81	0.10
	1.6	7.69	0.18
	1.8	8.80	0.21
	2	9.92	0.25
AR153	1	2.38	0
	1.2	3.40	0.28
	1.3	3.69	0.36
	1.45	3.94	0.43
	1.6	4.02	0.45
	1.85	4.13	0.48
	2	4.15	0.49

In Figure 18, the fitted value of $\Gamma_{||}$ does not show the predicted linear variation as a function of $\lambda - 1$. Actually, a linear variation with the initial experimental slope would make $S(q)$ diverge as soon as $\lambda \sim 1.4$. Because such a strain-induced spinodal decomposition is not observed, the fitted $\Gamma_{||}$ has to be kept below the decomposition limit and reaches a sort of plateau.

Rewriting eq 21 into a Lorentzian shape $S(q) = S(q\to 0)/(1 + q^2\xi_{||}^2)$, the model leads to a correlation length in the parallel direction

$$\xi_{RB||}^2 = \frac{\xi_0^2}{1 - 2\Gamma_{||}} \qquad (22)$$

A forced fit to a Lorentzian shape leads to values of $\xi_{RB||}$ which are "plateauing" as a function of λ (similarly to the variation of Γ). This disagrees with experiment, for which $\xi_{||}$ increases continuously with λ (Figure 13a). $\xi_{||}$ becomes larger than $\xi_{RB||}$; therefore the experimental curve is much steeper at low q than the forced fit,

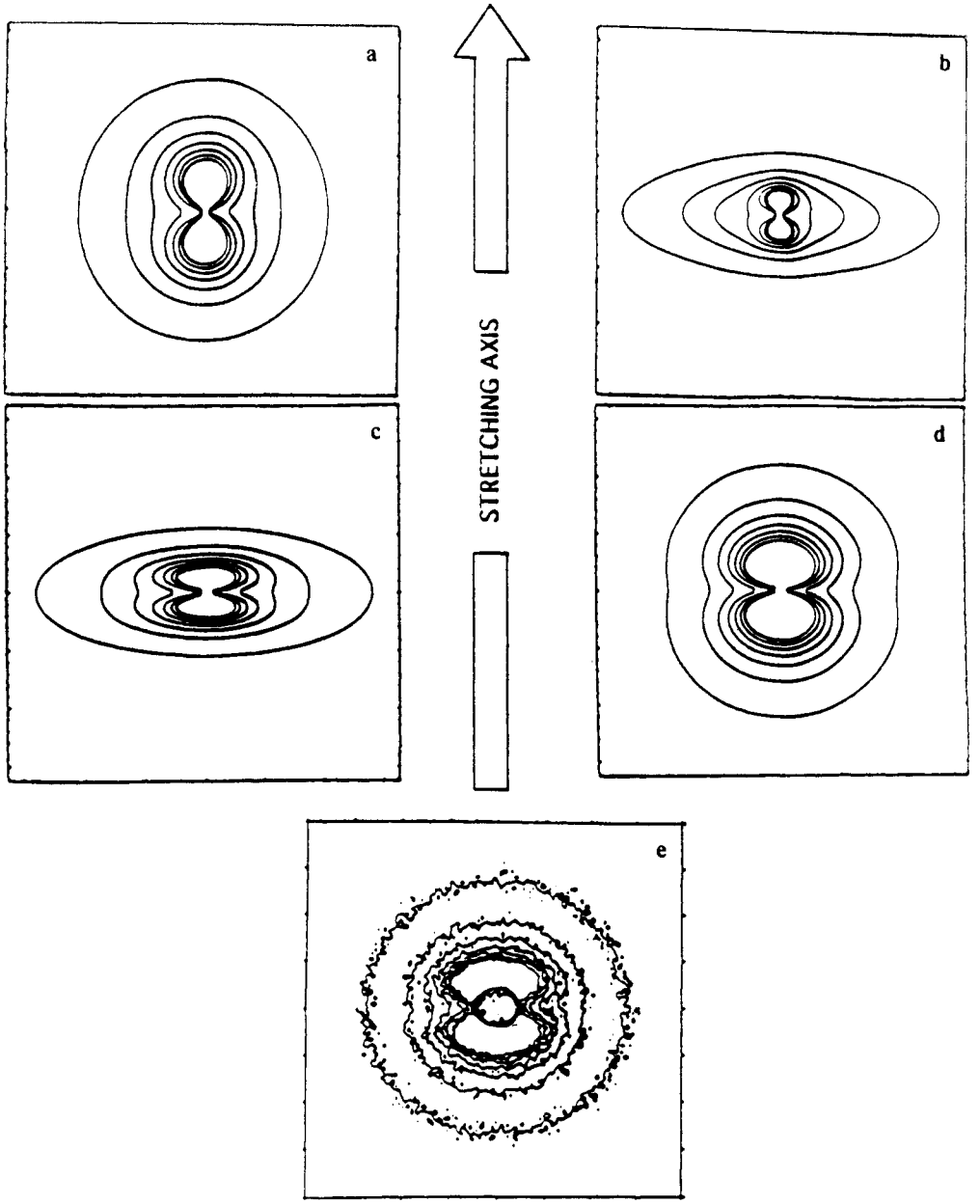

Figure 19. Comparison between the experimental isointensity contours (e) for sample AR143 after a relaxation time of 10 min at 134 °C for the elongation ratio $\lambda = 2$ and the calculated curves using (a) the genuine model corresponding to eq 21 (see ref 9), (b) affine deformation of the intrachain form factor (eq 23), (c) affine deformation of the intra- and interchain form factor (eq 24), and (d) affine deformation of the interchain form factor (eq 25).

leading to the "40% difference" at intermediate q reported for Figure 17.

In the perpendicular direction, $\Gamma(3\cos^2\psi - 1)$ is negative. Instead of approaching zero as in the parallel direction, the denominator increases further away from zero. $S(q)$ decreases more slowly when λ increases. However, it appears still too fast compared to the experimental behavior (unless the latter is smeared by radial averaging on a too wide sector).

We can also compare the shape of the isointensity patterns. The contours calculated with eq 21 do not depend on λ (Figure 19a). On the contrary the experimental curves (Figure 9) have wings of increasing ellipticity, at least from $\lambda = 1$ to 1.8 (a little variation of the shape is observed above 1.8). Introducing a classical deformation of the chains in eq 21, isointensity contours have been computed using

$$S(q) \cong \frac{1}{1 + (\lambda_{\parallel}^2 q_{\parallel}^2 + \lambda_{\perp}^2 q_{\perp}^2)\xi_0^2 - \Gamma(3\cos^2\psi - 1)} \tag{23}$$

Such a strong assumption (both the network ($S_{1H}(q)$) and the trapped chains ($S_{1D}(q)$) are deformed affinely at all scales) is not enough to produce butterflies with elliptical wings (see Figure 19b). Then we assume an affine deformation also for the term responsible for the butterfly shape,

$$S(q) \cong \frac{1}{1 + (\lambda_{\parallel}^2 q_{\parallel}^2 + \lambda_{\perp}^2 q_{\perp}^2)\xi_0^2 - \Gamma\left(\dfrac{3\lambda_{\parallel}^2 q_{\parallel}^2}{\lambda_{\parallel}^2 q_{\parallel}^2 + \lambda_{\perp}^2 q_{\perp}^2} - 1\right)} \tag{24}$$

which leads to Figure 19c, closer to the data. Finally, an affine deformation of the Γ term only gives

$$S(q) \cong \frac{1}{1 + q^2\xi_0^2 - \Gamma\left(\frac{3\lambda_\parallel^2 q_\parallel^2}{\lambda_\parallel^2 q_\parallel^2 + \lambda_\perp^2 q_\perp^2} - 1\right)} \quad (25)$$

which is the closest to experiment (Figure 19d). Thus the model would give a better description of the data if a deformation of the "superstructure" produced by the energy minimization is assumed.

For the same reasons, the value of the azimuthal angle ψ at which the scattering is the closest to the isotropic scattering varies with λ. As seen in Figure 10, the predicted value, $\tilde{\psi} = 55°$, at which $(3\cos^2\tilde{\psi} - 1) = 0$, is valid only if $\lambda \leq 1.3$. For larger λ, such a direction is closer to the "magic" angle, $\psi^*(\lambda)$, at which we have

$$J(\psi^*) = 1 \quad (26)$$

In this direction $\psi^*(\lambda)$, classical models[18-21] predict no deformation; $\tilde{\psi}$ is actually the limit of ψ^* when $\lambda \to 1$. For $\lambda = 2$, $\psi^* = 68°$; the ratio $I_{\psi^*}(q\to 0)/I_{iso}(q\to 0)$ is 1.11. This is much less than the ratio $I_\parallel(q\to 0)/I_{iso}(q\to 0) = 5$, but slightly higher than 1. To reach 1, one needs to consider a larger angle (i.e., a value of ψ^* for a larger λ, which can be found consistent with the exponent of the variation of ξ with λ, greater than one).

In summary, we observe several discrepancies with the predictions of the model of "amplification of spontaneous fluctuation", mostly linked to the large deformations studied here. Hydrodynamic models developed similarly for polymer solutions under shear[10,11] could lead to the same discrepancies.

4.4. "Cluster-like Heterogeneities" Model:[12,45,46] The Isotropic Case. In this model, the fluctuations in the cross-linking density are frozen, but at variance with the Onuki model,[13] they are not treated as a perturbation. They are assumed to form a sort of "superstructure", with respect to the mesh size, which can become progressively more "visible" under swelling by a mobile species, or stretching, in a scattering experiment.

We recall first the model developed for a very particular case, the random cross-linking of a semidilute solution. The latter is represented before cross-linking as a compact assembly of "blobs" (of size ξ_b, the correlation length), each one containing a nonentangled chain segment.[26] The random cross-linking is described as a site percolation process over the interchain contact points. This leads to clusters of blods cross-linked together, which we call "frozen blobs".

Under swelling, only regions poor in cross-links (where many "normal blobs" remain) will rearrange into larger blobs. The frozen blob clusters, which should deform less, can be viewed as "islands" in a "sea" of less concentrated material. They are "revealed" for the scattering, owing to a twofold mechanism: (i) increase in "contrast" (higher concentration out of the clusters) (ii) "unscreening" of correlations (larger spatial separation between the clusters, and as a result intracluster correlations are no longer screened out by intercluster correlations).

When one is close to the percolation threshold, such a process is simple to map on the dilution of the true percolation branched polymer cluster. One can indeed define a percolation threshold for the frozen blobs (one cross-link per blob). Using the result of Daoud and Leibler,[47] the scattering of the "quenched" fluctuations of concentration is expected to be Lorentzian for $q < \xi^{-1}$:

$$S(q) = S(q\to 0)/(1 + q^2\xi^2) \quad (27a)$$

$$S(q\to 0) \sim \phi^{-5/3} \quad (27b)$$

$$\xi \sim \phi^{-5/3} \quad (27c)$$

and to crossover toward a power law in an "intermediate q regime" for $\xi^{-1} < q < \xi_{sd}^{-1}$:

$$S(q > 1/\xi) \sim q^{-8/5} \quad (28)$$

ξ_{sd} is the correlation length of a semidilute solution of the same polymer concentration as that of the gel.

The exponent $8/5 = 1.6 = D_f(3 - \tau)$ is a combination of the true fractal dimension, $D_f = 2$ for one percolation cluster expanded by the excluded volume, and of τ, which characterizes the distribution of sizes of the clusters, $p(M) \sim M^{-\tau}f[(M/M_z)^\sigma]$.[47] M_z is the z-average of the molecular weight.

The strong concentration dependences of eqs 27b and 27c are due to the fact that the small clusters progressively leave the holes of the larger clusters where they were nesting. These holes are progressively revealed (or "unscreened") at larger and larger scales inside larger and larger clusters. Becoming quite large under swelling, the intensity from the frozen heterogeneities may easily dominate the scattering. The variations given by eqs 27a–c were effectively observed in swollen gels, in particular for gels prepared using the same cross-linking method[2] as in this paper but for particular degrees of cross-linking.[3] Exponents were weaker for some other degrees, which one could assume to be further from the percolation threshold.

However, the above model should not apply directly to the situation considered here. First, there are no obvious "frozen blobs" in these networks, since a large part of the cross-linking is achieved in the bulk after drying. Second, the network is only *slightly* swollen with *polymer chains* and not by a good solvent of low molecular weight.

We consider, for simplicity, a situation where the free chains are introduced after the network is formed. The main point that we want to keep is that a process, here cross-linking, which is entirely random but "frozen", can nevertheless (like percolation does) create clusters. Such a situation may also occur even if there is no definite percolation threshold. At the same time, the correlations should, again because of the randomness of their formation, remain essentially undetectable for a scattering experiment and become visible only after swelling or (see below) deformation. Let us associate a "height"[46] to the cross-linking density which fluctuates randomly in space (on distances larger than a certain correlation length) with a significant amplitude. Since polymer chains have a very low entropy of mixing, they should fill preferably the "valleys" in this random landscape. This is comparable to the islands formed as the sea invades a mountainous region. If the landscape is formed from a random process, the islands have the shape of percolation clusters and their size will frequently be larger than the correlation length of the "heights". Similarly, one may imagine that the partition of the free chains defines, by contrast, some branched percolation-like clusters. In Figure 20, we have arbitrarily chosen a threshold value X^* of cross-linking density, above which no chains penetrate (represented in black; we remind that for a binary incompressible mixture, it is equivalent to consider the free chains, or the "clusters", as the labeled objects carrying the cor-

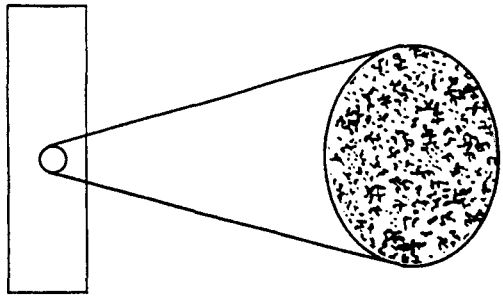

Figure 20. Schematic representation of random cross-linking heterogeneities in the network (the clusters (blackened areas) represent the regions where the cross-linking density is higher than average, and the free chains are concentrated in the white areas).

relations). Depending on X^*, such a picture will represent clusters more or less close to percolate. Though we do not known how the threshold is determined in the system, we assume that we remain close to a percolation situation.

Two extreme situations are considered:

A first possible one is that the labeled chains are expelled from all the clusters of the distribution. The fractal dimension, D_f, of the clusters should be equal here to 2.5, since, for a polymeric solvent, the cluster arms should not be expanded by excluded volume. Since $3 - \tau = 0.8$, one expects for the "intermediate regime" of q, such as $1/\xi < q < 1/R_g$

$$S(q) \sim q^{-D_f(3-\tau)} \sim q^{-2} \tag{29}$$

A second possible situation is that the chains are expelled from the inside of the larger clusters only, but not from clusters with a size comparable with their radius of gyration. In this case, polydispersity effects should be totally removed. Then, the contribution of the exponent τ vanishes, and

$$S(q) \sim q^{-D_f} \sim q^{-2.5} \tag{30}$$

Such a possibility has been invoked in order to explain a $1/q^{2.5}$ found in the scattering from radicalar PMMA-*co*-EDMA gels containing linear labeled chains.[48]

For the data of this paper, an intermediate regime of a power law type, different from that of the chains themselves, is not seen in Figure 2a, 3, and 4. Note that the q range should be $1/\xi < q < 1/R_{gD}$. A minimum value of ξ would be in the absence of free chains the average distance between two cross-links, not very different from the radius R_{gD} of the free chains. After the low swelling due to the introduction of the free chains, ξ is expected to be eventually only slightly larger than R_g. Consequently, one expects the scattered intensity to be slightly larger than that of an ideal mixture, as observed.

In Figure 2b, where the cross-linking ratio is varied on a much wider range, a different picture appears. For the lowest cross-linking, the behavior is almost similar to that just described with now, possibly, the beginning of a regime of a power law dependence with slopes varying between 2 and 2.5 (that is, different flow that of ideal chains). For the two larger cross-linking densities, a stronger increase in scattering is observed at low q accompanied by power law dependences with maximum slopes equal to 3 and 3.7. This could be explained by a progressive evolution between two regimes. First, as the cross-linking density is increased, the scattering first reaches a sort of limit curve, valid for a certain range of cross-linking and typical of the revealing of the heterogeneities by a soft partition of the free chains. Second, at the upper limit of this range, real separation should take place and make the scattering close to a q^{-4} Porod variation (sharp interfaces).

Such a q^{-4} signal is recorded when the host and the guest polymer are chemically different and immiscible. The guest can be either linear[46] or cross-linked (IPN's).[49] It was observed for these systems that the characteristic maximum size decreases as the average cross-linking density is increased. This is a situation for which the scattering decreases as predicted by eq 14, but it occurs only above the threshold of true phase separation.

In summary, we find that the increase in the scattering is in qualitative agreement with the presence of cross-linking heterogeneities, but no quantitative description is achieved.

4.5. "Cluster-like Heterogeneities" Model:[12,45,46] The Anisotropic Case. The model can be extended to the case of mechanical extension[12] by inverting the classical description of the swelling as a stretching in the three directions of space. The linear dilation of the gel under swelling is proportinal to $\phi^{-1/3}$. An extension by a factor λ in one direction can then be viewed as a change in "equivalent" polymer concentration, ϕ_{eq}, writing $\lambda \sim \phi_{eq}^{-1/3}$. Thus, the variation law $\xi \sim \phi^{-5/3}$ is transformed for the parallel direction into

$$\xi_{||} \sim \lambda^{3(5/3)} \sim \lambda^5 \tag{31}$$

which means that $S_{||}(q \to 0)$ also is strongly enhanced. Along the perpendicular direction, the sample is compressed by a factor $\lambda^{-1/2}$ (because of the conservation of volume). Therefore, one expects $\xi_\perp \sim (\lambda^{-1/2})^5 \sim \lambda^{-5/2}$, together with a decrease in $S_\perp(q \to 0)$. Using the same method, the scattering for any angle ψ can be computed, which leads to "butterfly" contour patterns. Experimentally, it was found that swollen gels under uniaxial extension exhibit butterfly patterns involving large variations of $\xi_{||}$ with λ. However, the observed exponents on fitting the results with an apparent scaling law remained smaller than 5 (one found $\cong 2$ or $\cong 3$ depending on the swelling ratio at which the stretching was performed). Such a lower effective exponent could be due to the fact that the clusters of frozen blobs are not only separated from each other as assumed in eq 31 but also stretched.

We now apply the same ideas to the system studied here, under uniaxial deformation. Similarly, the cluster-like islands, less deformed than the average, should separate in space along the stretching direction and interpenetrate more in the perpendicular direction. This should again lead to an "unscreening" process in the parallel direction: the nearly exact compensation of the intraisland correlations by the interisland correlations should progressively break down. $\xi_{||}$ and $S_{||}(q \to 0)$ should increase. The shift of $\xi_{||}$ with deformation should enlarge progressively the domain $1/\xi_{||} < q < 1/R_g$ and reveal the "intermediate behavior" of scattering. This would give rise to a pseudo "limit curve" on which the scattering curves corresponding to different elongations meet. The simplest prediction for this intermediate behavior, or "limit curve", would be

$$S(q) \sim q^{-D_{eff}} \qquad \text{for } 1/\xi_{||} < q < 1/R_g \tag{32}$$

D_{eff} being an "effective" fractal exponent intermediate between the values given by eqs 29 and 30. However,

partial deformation of the clusters may also act on D_{eff} or even make a true scaling behavior break down.

Equation 32 is consistent with the experimental behavior for the larger free chains, namely, the fact that the scattering curves for different extensions collapse progressively on a single curve, which can be approximated by a power law $I(q) \sim q^{-2.5}$ or $q^{-2.2}$ (depending on the samples). The values of these apparent exponents are moreover consistent with a structure of percolation clusters for the "islands", assuming that the polydispersity effects are entirely (exponent 2.5) or partly (exponent between 2 and 2.5) removed by the partitioning of the free chains. As mentioned above, the labeled free chains could be essentially expelled from the inside of the larger clusters. Therefore, the resulting "contrast" would reveal the latter only. Another explanation for this exponent 2.5 might be that the fluctuations are large enough to produce an onset of phase separation, increasing the apparent exponent. This picture is, however, not well supported by the relatively stable values observed for different samples and large λ's. For the shorter free chains (M_{WD} = 14 370), no such exponents are observed, no limit curve is clearly visible, and the only apparent slope in the intermediate regime is 1.13. In the framework of this model, this result can be explained by a weaker partition of the mobile species, because of their larger entropy of mixing.

Regarding the variation of ξ and $S(q\rightarrow 0)$, it is very difficult to make quantitative predictions in the parallel direction. First, the variations of ξ and $S(q\rightarrow 0)$ for the dilution of percolation clusters in the absence of excluded volume are not known. It could be

$$\xi \sim \phi^m$$

$$S(q\rightarrow 0) \sim \phi\xi^{D_{eff}} \sim \phi^{mD_{eff}+1} \qquad (33)$$

where m instead of being equal to 5/3 lies between 1 (corresponding to the dilution of monodisperse clusters with no excluded volume) and 2 (corresponding to the dilution of polydisperse percolation clusters with no excluded volume). As in the case of the stretched swollen gels (eq 31), stretching would lead to $\xi_{||} \sim \lambda^{3m}$ and to $S_{||}(q\rightarrow 0) \sim \lambda^{3mD_{eff}}$. However, the assumption of naught deformation for the cluster-like islands is undoubtedly too strong. If they are deformed by a factor λ_c, less than the macroscopic deformation λ, their separation in space would be roughly λ/λ_c instead of λ and one may expect $\xi_{||} \sim (\lambda/\lambda_c)^{3m}$. Then it is tempting to write $S_{||}(q\rightarrow 0) \sim (\lambda/\lambda_c)^{3mD_{eff}}$, which leads, even if λ_c and m are unknown, to the relation $S_{||}(q\rightarrow 0) \sim \xi_{||}^{D_{eff}}$. However, if the clusters are deformed, they should in principle lose their fractal character, because the deformation should not be scale invariant. For example, an ideal linear chain is a fractal, but not an ideal chain stretched by its extremties. Therefore, a true scaling behavior, $S(q) \sim q^{-D_{eff}}$, for $1/\xi_{||} < q < 1/R_g$ could be incompletely reached. This deviation could remain limited to the low-q range. By analogy with the loss of the affinity for small distances along an end-to-end pulled linear chain, the smaller clusters should not be concerned. Then, the limit curve would still be observed for the larger q of the "intermediate regime".

Experimentally, the largest variation of $\xi_{||}$ found for large free chains is $\xi_{||} \sim \lambda^{2.28}$, slightly weaker, and the other sample gives us $\xi_{||} \sim \lambda^{1.98}$, which lies well below the simple prediction. Finally, for the short free chains, the variation is much weaker ($\xi_{||} \sim \lambda^{1.27}$). Besides, a simple scaling picture should lead to $S_{||}(q\rightarrow 0) \sim \xi_{||}^{D_{eff}}$. In the present experiments, for sample AR143, we get $S_{||}(q\rightarrow 0) \sim \xi_{||}^{D'}$, where $D' \approx 1.94$ is slightly smaller than $D_{eff} \approx 2.5$ and for sample AR153, we get $D' \approx 2.09$, relatively close to $D_{eff} \approx 2.2$. Thus the experimentally observed effects are a bit softer than the estimated ones assuming no deformation of the clusters, which may be unrealistic.

In the perpendicular direction, the reverse effect should, in principle, occur: the cluster-like islands should reinterpenetrate, from the state of slight separation produced by the incorporation of the free chains. As a result, both the correlation length, $\xi_\perp$ and the scattering intensity at low q should decrease upon stretching at the expense of the scattering in the intermediate regime, $1/\xi_\perp < q < 1/R_g$, which should vanish at some point. Then, the decrease of the intensity with elongation should either stop and remain at the level it reached (nearly that of an un-cross-linked melt because the intracluster correlations should be perfectly screened out), which is exactly what is observed, or, possibly, reincrease, because the ideal screening conditions would again be lost, which is not observed, except for a small effect at the lowest q.

In summary, this picture of cluster-like heterogeneities does not predict quantitatively the change under strain of the correlation length ξ and the extrapolated intensity I_0. However, it is the only model to predict (i) a large effect of the strain of the correlation length and (ii) the appearance, and the enlargement under strain, of an "intermediate regime" of scattering (with a scaling dependence of $I(q)$), both characteristics of the experimental curves reported here. Moreover, applying the same idea to any direction ψ and replacing λ by λ_{eff} as defined above will also lead to the same limit curve, as observed experimentally. Consequently, the elliptical shape of the wings of the butterfly patterns will be very close to those observed, at variance with the other models.

5. Summary and Conclusions

The scattering from networks containing deuterated un-cross-linked small chains, at rest and under deformation has been measured. Two values for the cross-linking ratio and two values for the molecular weight M_{WD} of the small un-cross-linked chains have been chosen. In the *isotropic state*, the cross-linking increases the scattering with respect to random mixing, and this effect increases with the cross-linking ratio. The effect is visible for small and large M_{WD} but increases strongly on passing from the lower (14 370) to the larger value (73 000). In the *deformed state*, the scattering increases continuously in the parallel direction and in intermediate directions corresponding to a dilatation of the sample along this direction. In the perpendicular direction, corresponding to a contraction, the scattering slightly decreases compared to the isotropic state and then stabilizes around the random mixing value. We are, however, disturbed by the smearing effect due to radial averaging over too-wide angular sectors, necessary for reasonably large enough intensity, for large λ. Butterfly patterns are observed along the parallel direction, corresponding to a larger scattering in the parallel than in the perpendicular direction even at $q \rightarrow 0$.

Comparison with classical models of the RPA type, describing the mixing of elongated chains under the effect of cross-linking, leads to strong disagreement, since ellipses or butterflies both with the great axes

perpendicular to the stretching are predicted. Recent linear elasticity calculations are closer to the data, by assuming spontaneous (thermal) or frozen fluctuations, leading, after minimization of the elastic and mixing free energy, to larger fluctuations in the parallel direction, even at $q \to 0$. However, the variations in I_0 and ξ, allowing one to adjust the data to a Lorentzian shape, disagree with these models. In the case of the amplification under strain of the spontaneous (thermal) fluctuations,[9] the intensity should overshoot at large λ, which is not observed. A more refined version, including new nonlinear terms, should be checked. For the perturbation model of uncorrelated frozen fluctuations[13] (eq 17), the correlation length is predicted to be stable, which is not observed experimentally, and the predicted variation of the frozen contribution is too strong as λ is increased. This model could be reinfed by introducing correlations for the frozen heterogeneities. This would be very near to the last model discussed, which assumes that the increase in scattering is due to an "unscreening" effect associated with the separation, under cross-linking and deformation, of percolation-like clusters. This model predicts, as observed, the appearance and the enlargement under strain of an intermediate scattering regime, characterized by a power law dependence of $I(q)$ with q. It also predicts, as observed, power law dependences for I_0 and ξ as a function of λ. The values of exponents measured in the latter cases are smaller than those which can be estimated in a simple way. Even at the present stage, this model gives the best prediction of the basic features of the scattering curves.

Finally, the strong resemblance between the system studied here—networks with mobile chains—with two other systems is stressed: (i) networks with solvent and (ii) long entangled chains (a temporary network) mixed with smaller chains (relaxing and diffusing faster). Under strain, such systems exhibit similar butterfly patterns. Comparable patterns were also observed recently, using light scattering, in the cases of simple-sheared solutions[5,6] and of pure-sheared blends close to demixing.[7] Some of these experiments received an explanation in terms of hydrodynamic models[10,11] which we believe to be close to the spontaneous fluctuation model, btu a heterogeneity model could also qualitatively account for the results.[46] It would, however, be necessary in such cases of entangled solutions and entangled melts to understand the origin of entanglement heterogeneities, which are more difficult to explain than the cross-linking heterogeneities.

Acknowledgment. We are grateful to C. Hayes for kindly reviewing the manuscript, and we thank A. Lapp for the measurements of the molecular weight distribution of the polymers.

Appendix. Linear Elasticity Theory: Homogeneous and Heterogeneous Cases

The starting point is the free energy:[13,17,26,41]

$$\Delta F = \frac{1}{2}K_{\text{gel}}^{\text{osm}}\left(\sum_i u_{ii}\right)^2 + \mu\sum_i\sum_k\left(u_{ik} - \frac{1}{3}\delta_{ik}\sum_i u_{ii}\right)^2 + M(\nabla\phi)^2 \quad \text{(A-1)}$$

where $\vec{u}$ is the displacement with respect to the position in the "reference state" (concentration $\phi = \phi_0$) in which the network is *assumed* to be at rest. $u_{ik} = (1/2)(\partial u_i/\partial x_k + \partial u_k/\partial x_i)$, with $i,k = x$, y, or z, $K_{\text{osm}} = \phi^2(\partial^2\Delta F/\partial\phi^2)$ is the osmotic modulus, μ is the shear modulus, and M is a constant. The change in concentration with respect to ϕ_0 is given as $\delta\phi/\phi_0 \cong -\sum_i u_{ii} = -\text{div}\ \vec{u}$. The displacement, $\vec{u}$, is assumed to be small. For a large change in volume or a high elongation ratio, u_{ik} should be replaced by $\lambda_{ik} = \partial X_i/\partial x_k^\circ$, where $x_0 = (x_x^\circ, x_y^\circ, x_z^\circ)$ are the Cartesian coordinates in some reference relaxed state representing the original position before deformation and $X = (X_x, X_y, X_z)$ are those of the deformed gel representing the real spatial position.[13] This allows also one to define the elastic free energy of deformation for a Gaussian network:

$$\Delta F_{\text{el}} = \frac{1}{2}k_B T\nu_0\left(\frac{\phi}{\phi_0}\right)\sum_i\sum_k\left(\frac{\partial X_i}{\partial x_k^\circ}\right)^2 \quad \text{(A-2)}$$

In the swelling case, the gel is isotropically expanded; hence

$$\frac{\partial X_i}{\partial x_k^\circ} = \delta_{ik}\left(\frac{\phi}{\phi_0}\right)^{-1/3} \quad \text{(A-3)}$$

References and Notes

(1) (a) Oeser, R.; Picot, C.; Herz, J. In *Polymer Motion in Dense Systems*; Richter, D., Springer, T., Eds.; Springer Proceedings in Physics 29; Springer-Verlag: Berlin, 1988; p 104. (b) Oeser, R. Thesis, University of Mainz, Germany, 1992.
(2) (a) Zielinski, F.; Buzier, M.; Lartigue, C.; Bastide, J.; Boué, F. *Prog. Colloid. Polym. Sci.* **1992**, *90*, 115. (b) Zielinski, F. Thesis, Université Pierre et Marie Curie, Paris VI, France, 1991.
(3) (a) Mendes, E. Thesis, Université Louis Pasteur, Strasbourg, France, 1991. (b) Mendes, E.; Lindner, P.; Buzier, M.; Boué, F.; Bastide, J. *Phys. Rev. Lett.* **1991**, *66*, 1595.
(4) Bastide, J.; Buzier, M.; Boué, F. In *Polymer Motion in Dense Systems*; Richter, D., Springer, T., Eds.; Springer Proceedings in Physics 29; Springer-Verlag: Berlin, 1988; p 112.
(5) Hashimoto, T.; Kume, T. *J. Jp. Soc. Phys.* **1992**, *61*, 1839.
(6) Wu, X. L.; Pine, D. J.; Dixon, P. K. *Phys. Rev. Lett.* **1991**, *68*, 2408.
(7) (a) Van Egmond, J. W.; Werner, D. E.; Fuller, G. G. *J. Chem. Phys.* **1992**, *96*, 7742. (b) Fuller, G. G. *Rheol. Acta* **1991**, *30*, 89.
(8) Boué, F.; Lindner, P., submitted for publication.
(9) Rabin, Y.; Bruinsma, R. *Europhys. Lett.* **1992**, *20*, 79.
(10) Fredrickson, G. H.; Helfand, E. H. *Phys. Rev. Lett.* **1989**, *62*, 2468.
(11) Milner, S. T. *Phys. Rev. Lett.* **1991**, *66*, 1477.
(12) Bastide, J.; Leibler, L.; Prost, J. *Macromolecules* **1990**, *23*, 1821.
(13) Onuki, A. *J. Phys. II* **1992**, *2*, 45.
(14) Williams, M. L.; Landel, R. F.; Ferry, J. D. *J. Chem. Phys.* **1955**, 3161.
(15) Ferry, J. D. *Viscoelastic Properties of Polymers*; John Wiley and Sons: New York, 1980.
(16) Treloar, L. R. G. *The Physics of Rubber Elasticity*; Clarendon Press: Oxford, 1940.
(17) Landau, L. D.; Lifshitz, E. M. *Theory of Elasticity*; Pergamon Press: Oxford, 1986.
(18) Kuhn, W. *Kolloid Z.* **1939**, *87*, 3.
(19) Wall, F. T.; Flory, P. J. *J. Chem. Phys.* **1951**, *19*, 1435.
(20) Flory, P. J. *Principles of Polymer Chemistry*; Cornell University Press: Ithaca, NY, 1953.
(21) Mark, J. E.; Sullivan, J. L. *J. Chem. Phys.* **1979**, *70*, 1794.
(22) Flory, P. J.; Tatara, Y. J. *Polymer* **1975**, *13*, 683.
(23) Cotton, J. P. In *Neutron, X-Ray and Light Scattering*; Lindner, P., Zemb, T., Eds.; Elsevier: Amsterdam, 1991.
(24) Boué, F.; Nierlich, M.; Jannink, G.; Ball, R. C. *J. Phys. Lett.* **1982**, *43*, L-589.
(25) Boué, F. *Adv. Polym. Sci.* **1987**, *82*, 47.
(26) de Gennes, P.-G. *Scaling Concepts in Polymer Physics*; Cornell University Press: Ithaca, NY, 1979.
(27) Bates, F. S.; Wignall, G. D. *Macromolecules* **1986**, *19*, 932.
(28) Briber, R.; Bauer, R. *Macromolecules* **1991**, *24*, 1899.
(29) The Zimm plots obtained in ref 28 were more linear. This may be partly due to a slightly narrower q range, inside which our results look more linear, and may be also due to the difference in the cross-linking methods.

(30) In practice, butterfly patterns appeared at very low temperatures, $T < 100$ °C. It seems therefore that the T_g (approximately 100 °C) was slightly shifted toward lower values by traces of solvent remaining in the sample. The T_g is estimated to be around 90 °C from the variation of the force during stretching and relaxation.
(31) (a) Ramzi, A.; Zielinski, F.; Hakiki, A.; Buzier, M.; Bastide, J.; Boué, F. 204th National Meeting of the American Chemical Society, August 1992, p 229. (b) Ramzi, A.; Mendes, E.; Zielinski, F.; Rouf, C.; Hakiki, A.; Herz, J.; Oeser, R.; Boué, F.; Bastide, J. *J. Phys. IV* **1993**, *3*, 91.
(32) Mark, J. E. *Rubber Chem. Technol.* **1975**, *48*, 495.
(33) Mooney, M. *J. Appl. Phys.* **1948**, *19*, 434.
(34) Rivlin, R. S. *Philos. Trans. R. Soc. London* **1948**, *A241*, 379.
(35) Rivlin, R. S. *J. Appl. Phys.* **1948**, *18*, 444.
(36) James, H.; Guth, E. *J. Chem. Phys.* **1951**, *19*, 1435.
(37) Flory, P. J. *Proc. R. Soc., London* **1976**, *351*, 351.
(38) Graessley, W. W. *Macromolecules* **1975**, *8*, 186.
(39) Graessley, W. W. *Macromolecules* **1975**, *8*, 865.
(40) Boué, F.; Bastide, J.; Buzier, M.; Collette, C.; Lapp, A.; Herz, J. *Prog. Colloid Polym. Sci.* **1987**, *75*, 152.
(41) Tanaka, T.; Hocker, L. O.; Benedek, G. B. *J. Chem. Phys.* **1973**, *59*, 5151.
(42) Horkay, F.; Heckt, A.-M.; Geissler, E. *J. Chem. Phys.* **1989**, *91*, 2706.
(43) Onuki, A. Instabilities and Patterns in Elastic Materials: Gels and Solid Solutions. In *Formation, Dynamics, and Statistics of Patterns*; Kawasaki, K., et al., Eds.; World Scientific: Singapore, 1990.
(44) Rabin, Y.; Onuki, A. *Macromolecules* **1994**, *27*, 870.
(45) Bastide, J.; Boué, F.; Mendes, E.; Zielinski, F.; Buzier, M.; Beinert, G.; Oeser, R.; Lartigue, C. *Networks 91*; Dusek, K., Kuchanov, S. I., The Netherlands, 1992, p 119.
(46) Bastide, J.; Boué, F.; Oeser, R.; Mendes, E.; Zielinski, F.; Buzier, M.; Lartigue, C.; Lindner, P. *Mater. Res. Soc. Symp. Proc.* **1992**, *248*, 313.
(47) Daoud, M.; Leibler, L. *Macromolecules* **1988**, *21*, 1497.
(48) Lal, J.; Bastide, J.; Bansil, R.; Boué, F. *Macromolecules* **1993**, *26*, 6092.
(49) Lal, J.; Widmayer, J. M.; Bastide, J.; Boué, F., to be submitted.

MA946122R